bioRxiv preprint doi: https://doi.org/10.1101/047779; this version posted May 11, 2016. The copyright holder for this preprint (which was not certified by peer review) is the author/funder. All rights reserved. No reuse allowed without permission.

# Fluorescence resonance energy transfer and protein-induced fluorescence enhancement as synergetic multi-scale molecular rulers

*Evelyn Ploetz[1,# §], Eitan Lerner[2,#], Florence Husada[1], Martin Roelfs[1], Sangyoon Chung[2], Johannes Hohlbein[3,4], Shimon Weiss[2] and Thorben Cordes[1,*]*

[1] Molecular Microscopy Research Group, Zernike Institute for Advanced Materials, University of Groningen, Nijenborgh 4, 9747 AG Groningen, The Netherlands

[2] Department of Chemistry and Biochemistry, University of California Los Angeles, Los Angeles, CA 90095, USA

[3] Laboratory of Biophysics, Wageningen University and Research, Wageningen, The Netherlands

[4] Microspectroscopy Centre, Wageningen University and Research, Wageningen, The Netherlands

[§] Present address: Physical Chemistry, Department of Chemistry, Ludwig Maximilians-Universität München, 81377 Munich, Germany

# these authors contributed equally; *corresponding author, t.m.cordes@rug.nl

bioRxiv preprint doi: https://doi.org/10.1101/047779; this version posted May 11, 2016. The copyright holder for this preprint (which was not certified by peer review) is the author/funder. All rights reserved. No reuse allowed without permission.

## ABSTRACT

Advanced microscopy methods allow obtaining information on (dynamic) conformational changes in biomolecules via measuring a single molecular distance in the structure. It is, however, extremely challenging to capture the full depth of a three-dimensional biochemical state, binding-related structural changes or conformational cross-talk in multi-protein complexes using one-dimensional assays. In this paper we address this fundamental problem by extending the standard molecular ruler based on Förster resonance energy transfer (FRET) into a two-dimensional assay via its combination with protein-induced fluorescence enhancement (PIFE). We show that donor brightness (*via* PIFE) and energy transfer efficiency (*via* FRET) can simultaneously report on e.g., the conformational state of dsDNA following its interaction with unlabelled proteins (*Bam*HI, *Eco*RV, T7 DNA polymerase gp5/trx). The PIFE-FRET assay uses established labelling protocols and single molecule fluorescence detection schemes (alternating-laser excitation, ALEX). Besides quantitative studies of PIFE and FRET ruler characteristics, we outline possible applications of ALEX-based PIFE-FRET for single-molecule studies with diffusing and immobilized molecules. Finally, we study transcription initiation and scrunching of *E. Coli* RNA-polymerase with PIFE-FRET and provide direct evidence for the physical presence and vicinity of the polymerase that causes structural changes and scrunching of the transcriptional DNA bubble.

## INTRODUCTION

Advanced microscopy methods have become powerful tools for structural studies of biomolecules. These methods can complement classical biochemical and biophysical techniques[1,2], but most importantly emerged as key player in understanding structural dynamics[3,4]. The underlying biophysical concept is straight forward: Construct a one-dimensional molecular ruler, in which the biochemical state of the system can be read out as a distance-related measure. Such a molecular ruler often uses a photophysical property such as fluorophore brightness or lifetime to provide information on the structure of biomolecules in real time.[5]

bioRxiv preprint doi: https://doi.org/10.1101/047779; this version posted May 11, 2016. The copyright holder for this preprint (which was not certified by peer review) is the author/funder. All rights reserved. No reuse allowed without permission.

A classic example for such a molecular ruler is Förster resonance energy transfer (FRET)[5], which allows achieving a spatial resolution in the nanometre range with (sub)millisecond temporal resolution.[6-10]. However, other photophysical effects such as photo-induced electron transfer (PET)[11-14] or protein-induced fluorescence enhancement (PIFE)[15-19] can be used for similar purposes. Since the fluorescent signal can be read out with high time-resolution, even fast conformational changes[20-26], as well as interactions between biomolecules, can be mapped in physiologically relevant environments *in vitro* [27,28] and *in vivo*[29,30] with a sensitivity allowing to address individual molecules. These molecular rulers suffer from limitations such as their restricted distance ranges and the need for labelling with fluorescent dyes. Most importantly, in the assessment of a three-dimensional (dynamic) structure, the largest limitation is embedded in the information accessible to these methods, which at best follow a single distance to capture a complex structural state.

This restriction prohibits monitoring an essential feature of biological processes. While single distances can be read out with high spatio-temporal-resolution, it remains challenging to simultaneously observe conformational changes in different protein parts, map these structural changes as either a result of protein binding or due to intrinsic dynamics[31] and observe how multi-subunit proteins coordinate conformational changes between different domains. To tackle these problems, multiple distances need to be monitored simultaneously (as read-out for the respective biochemical states). Multi-colour approaches have been employede, e.g., FRET assays with more than two different fluorescent labels, but are not routinely used for complex biological systems due to difficulties in terms of physical instrumentation, molecular biology or labelling chemistry.[32-36]

In this paper, we combine two fluorescence-related effects into one powerful assay that we dub ALEX-based PIFE-FRET. It allows observing changes in biochemical structure and interactions by following two distances with two different distance dynamic ranges. Strikingly, ALEX-based PIFE-FRET requires labelling with only two fluorescent dyes, i.e., similar to FRET. Its enhanced information content is provided by use of additional photophysical parameters, which are extracted via advanced data analysis procedures using single-molecule fluorescence detection and alternating-laser

bioRxiv preprint doi: https://doi.org/10.1101/047779; this version posted May 11, 2016. The copyright holder for this preprint (which was not certified by peer review) is the author/funder. All rights reserved. No reuse allowed without permission.

excitation. In detail, we utilize the stoichiometry parameter, S, as a measure for PIFE-effects (which may report on the vicinity of a protein bound to a DNA duplex), while FRET reports on the distance between fluorophores (which may report on the global conformation that a DNA duplex adopts upon protein binding). PIFE-FRET does not necessarily require surface-immobilized biomolecular complexes and hence obviates the use of other complex techniques such as ABEL-trap [37,38], feedback loop tracking [39] or use of microfluidic devices[40].

To successfully construct and use a two-dimensional ruler thereby introducing PIFE for solution-based single-molecule experiments, we provide a framework for data analysis routine to allow simultaneous and quantitative read-out of two different photophysical parameters: donor brightness (PIFE) and energy transfer efficiency (FRET). In proof-of-concept experiments we study different oligonucleotide samples containing the environmentally sensitive donor Cy3 (PIFE fluorophore; FRET donor) in comparison to the fluorescence signals of the less environment-sensitive FRET donor Cy3B, combined with the acceptor ATTO647N. We show that PIFE-FRET enables the detection of the interaction between unlabelled proteins and doubly labelled diffusing dsDNA via changes in brightness ratio S (termed stoichiometry) using µs-ALEX[41]. We further investigated the spatial sensitivity of PIFE-FRET for binding of DNA-binding enzymes with respect to the PIFE- and FRET-ruler aspects. The modulation of donor-brightness due to PIFE (and hence the Förster radius) preserves the FRET-distance information after careful data evaluation. Finally, we study DNA scrunching in transcription initiation of *E. Coli* RNA-polymerase *(RNAP)*. Using PIFE-FRET, we provide the first direct evidence for simultaneous structural changes in the formed DNA bubble (→ DNA open bubble formation and DNA scrunching *via* FRET) accompanied by the physical presence of the RNAP protein (→the vicinity of the bound RNAP to the promoter DNA *via* PIFE). Interestingly, we were able to identify an extrusion of the nontemplate strand of the transcription bubble out of the active site, recently identified through classic footprinting experiments[42], yet without the use of chemical cross-linking reagents. The extrusion of the nontemplate strand was coupled to specific conformational changes in the bubble, caused by DNA scrunching. Lastly, we outline possible applications of PIFE-FRET both in studies with diffusing and immobilized

bioRxiv preprint doi: https://doi.org/10.1101/047779; this version posted May 11, 2016. The copyright holder for this preprint (which was not certified by peer review) is the author/funder. All rights reserved. No reuse allowed without permission.

molecules indicating the full potential of the technique for mechanistic investigations of biomolecular interactions.

## RESULTS

**The principles of ALEX-based PIFE-FRET.** The aim of the PIFE-FRET assay is to monitor two distances simultaneously with different dynamic ranges in complexes between proteins or nucleic acids and proteins. In the assay, we label two complementary ssDNA strands with donor (D) and acceptor (A) fluorophores both encoding distinct DNA binding sites after annealing (Fig. 1A). The brightness of the Cy3 donor fluorophore is increased upon binding of proteins in close proximity (Fig. 1C, PIFE), hence directly reports on the distance $R_1$ between fluorophore and the surface of the bound protein (Fig. 1A).

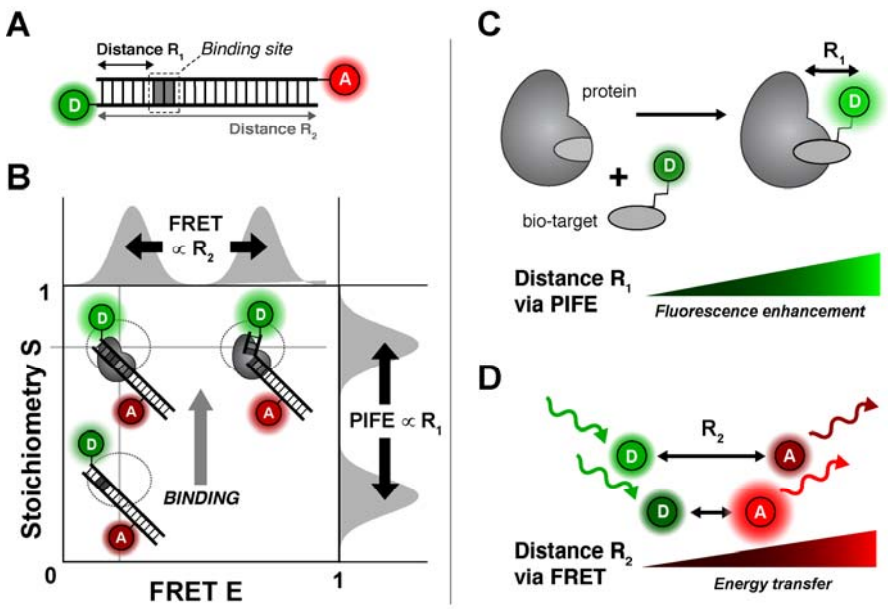


**Figure 1. Working principle of ALEX-based PIFE-FRET. (A)** Possible labelling scheme for PIFE-FRET experiments: a DNA template is labelled with FRET donor D and acceptor A and contains a binding site for a protein. **(B)** Read out of PIFE and FRET distances via ALEX: E-S-histogram depicts that changes of $R_2$ can be monitored via FRET efficiency E, whereas distance $R_1$ between donor and protein are determined by changes in stoichiometry S. **(C/D)** Photophysical effects reporting on distances $R_1$ and $R_2$: **(C)** PIFE reports on distance $R_1$ between donor and the surface of a bound protein via fluorophore brightness. **(D)** FRET between D and A reports on distance $R_2$.

bioRxiv preprint doi: https://doi.org/10.1101/047779; this version posted May 11, 2016. The copyright holder for this preprint (which was not certified by peer review) is the author/funder. All rights reserved. No reuse allowed without permission.

The conformation of dsDNA is monitored by FRET (Fig. 1D, FRET) via changes in the interprobe distance $R_2$ between D and A (Fig. 1A). A donor fluorophore that fulfils the requirements of the PIFE-FRET assay is the green cyanine dye Cy3 (Fig. S1), in which cis/trans excited-state isomerization competes directly with FRET on excitation energy in a dye microenvironment-dependent manner. Finally, an experimental technique is required for simultaneously reporting on both photophysical parameters. For this we suggest to use alternating laser excitation (ALEX), which reports on PIFE effects via the ratiometric parameters, stoichiometry, S, and FRET efficiency, E (Fig. 1B). Both parameters of ALEX can be used for mapping out PIFE-FRET since S is defined as brightness ratio between the donor and acceptor fluorophore (Eqn. 6) and is hence sensitive to PIFE (as long as the brightness of the acceptor fluorophore is stable and unchanging) while E compares only donor-excitation-based intensities to derive the FRET efficiency (Eqn. 3-4).

While the proposed assay and its implementation in ALEX is as a straightforward combination to increase the information content of PIFE and FRET, the interdependency of photophysical properties represents a fundamental hurdle and will therefore be addressed carefully. Since the green donor fluorophore is integral part of both rulers, both PIFE and FRET compete directly via non-radiative de-excitation of the donor (Fig. 2).

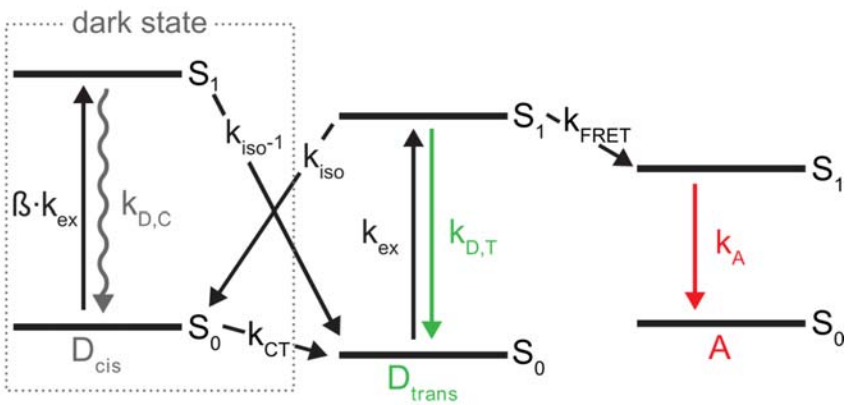


**Figure 2. Jablonski diagram of Cy3 in the presence of a FRET acceptor.** After excitation ($k_{ex}$) to the excited *trans* isomer ($D_{trans}$), three competing pathways deplete the excited state $S_1$: (a) $k_{D,T}$ which is the sum of radiative and non-radiative decay rates from $S_1$ to $S_0$ resulting in fluorescence emission; (b) trans to cis photo-isomerization with $k_{iso}$ resulting in the formation of the non-fluorescent *cis* isomer $D_{cis}$ of Cy3; (c) Förster-type energy transfer $k_{FRET}$ to an acceptor fluorophore A. The rates for Cy3 cis/trans

bioRxiv preprint doi: https://doi.org/10.1101/047779; this version posted May 11, 2016. The copyright holder for this preprint (which was not certified by peer review) is the author/funder. All rights reserved. No reuse allowed without permission.

isomerization $k_{iso}$ and $k_{iso}^{-1}$ are sensitive to the environment and are modulated by PIFE. ß accounts for differences in the extinction coefficients of cis and trans isomer at the excitation wavelength.

The quantum yield of Cy3 is environmentally sensitive, i.e., the PIFE effect alters both the non-radiative cis/trans isomerization ($k_{iso}$) and the FRET parameters (Förster radius, $R_0$ and hence the rate of energy transfer, $k_{FRET}$) without changes in the distance between the donor and the acceptor. We therefore first describe a photophysical model as well as present a procedure for data evaluation in order to decouple both effects and determine PIFE (distance $R_1$) and FRET (distance $R_2$) in one experiment using a ratiometric approach rather than fluorescence lifetimes of the donor fluorophore[43,44].

**Photophysics of PIFE-FRET.** The fluorophore Cy3 and similar cyanine fluorophores (DyLight 547, DyLight 647[45], Cy5, Alexa Fluor 647) have been employed for PIFE as they all share the property of excited-state cis/trans isomerization that leads to strong dependence of their fluorescence quantum yield with respect to the local environment.[46] This dependence includes the specific location of dye-attachment (for DNA 5'/3' vs. internal labelling) as well as three-dimensional structure (single- vs. double-stranded DNA).[46-48] The effect can be used to monitor interactions between an unlabeled protein and a fluorophore-labelled macromolecule (e.g., a dsDNA duplex Fig. 1C). Restricting the rotational freedom of the fluorophore by applying steric hindrance[49,50], the interacting protein causes an increase in fluorescence intensity without chromatic changes (Fig. S1). This effect allows the observation of complex formation between e.g., a Cy3-labelled oligonucleotide and a DNA-binding protein.[16] In special scenarios (i.e., where suitable calibration is possible) PIFE can even serve as a quantitative ruler to determine fluorophore–protein proximity at base-pair resolution in a distance range of up to 3 nm that is inaccessible to smFRET[43,44].

The underlying photophysical principle of PIFE was recently studied in detail by Levitus and co-workers[51]: The *trans* isomer of Cy3 is thermally stable, while the lifetime of non-fluorescent, ground-state *cis*-Cy3 is found in the µs range (Fig. 2, $k_{ct}$).[52] The de-excitation of isolated excited-state *trans*-Cy3 occurs primarily via two pathways, i.e., *cis*/*trans* isomerization with rate $k_{iso}$ and fluorescence with rate $k_{D,T}$ (Fig. 2)[53], Under typical single-molecule conditions, i.e., continuous green excitation, both isomers

bioRxiv preprint doi: https://doi.org/10.1101/047779; this version posted May 11, 2016. The copyright holder for this preprint (which was not certified by peer review) is the author/funder. All rights reserved. No reuse allowed without permission.

*cis*/*trans* are populated during a fixed time interval with a population distribution determined by the microenvironment, which mainly alters rates $k_{iso}$ and $k_{iso'}$ (Fig. 2). Both rates depend on the energetic barriers between the isomers in excited-state (and the rotational diffusivities for crossing them) between the corresponding $S_1$-minima and a 90°-twisted geometry of Cy3 (Fig. S1).[51] All other rates (except $k_{iso}$ and $k_{iso'}$) remain constant upon a change of the local environment. The PIFE effect of Cy3 corresponds to a change in the population distribution between *cis* and *trans* isomers, since it is mostly the trans isomer that contributes to a fluorescent signal (Fig. 2). Consequently, the mean fluorescence quantum yield, QY of Cy3 (not its spectrum, Fig. S2) varies with environmental polarity, steric hindrance, (micro)viscosity[48] and is thus sensitive to adjacent binding of biomolecules such as proteins or DNA. It was shown experimentally that the isomerization rate constants are altered mainly in their pre-exponential factors due to a stronger dependence on diffusivity[54]. It was also shown that *cis*/*trans*-isomerization can be fully blocked by creating structural rigidity as in the derivative Cy3B (Fig. S1), leading to strongly reduced environmental sensitivity and increased brightness.[46,55] Cy3B hence serves as a fluorophore that can emulate the maximal PIFE-effect since *cis*/*trans* isomerization is fully prohibited/abolished in this molecule. When PIFE is combined with FRET, the donor-excited state is altered by both changes in $k_{iso}$ and $k_{FRET}$, and both rulers are directly dependent of each other (Fig. 2), however a change in $k_{iso}$ is independent of the D-A distance $R_2$. Therefore, after applying corrections to account for the changes in the QY of the donor, one can elucidate both PIFE and FRET information.

**Characterization of PIFE-signatures in ALEX experiments.** In order to understand the experimental signature of PIFE in FRET assays, we compared the spectroscopic properties of Cy3 and Cy3B in bulk and single-molecule experiments. Bulk fluorescence measurements of Cy3(B) on dsDNA were performed in the presence of increasing concentrations of iodide. These experiments show how both Cy3 and Cy3B are collisionally quenched at the same iodide concentration scale (Figs. S1C/D). However, Stern-Volmer plots show that the fluorescence QY of Cy3B depends linearly on Iodide concentrations, whereas Cy3 shows a nonlinear relation that is characteristic for a

bioRxiv preprint doi: https://doi.org/10.1101/047779; this version posted May 11, 2016. The copyright holder for this preprint (which was not certified by peer review) is the author/funder. All rights reserved. No reuse allowed without permission.

system with a sub-populations of fluorophores accessible and inaccessible to the iodide quencher (Fig. S1E).[56] As expected, the relative QY of Cy3 further increased with increasing glycerol concentrations, whereas the relative QY of Cy3B is almost unaffected and remained constant under similar conditions (Figs. S1F/G). Increasing bulk viscosity of Cy3 affected fluorescence intensity with only negligible chromatic changes. These experiments suggest that PIFE effects indeed mainly influence the QY of Cy3 and hence the intensity of associated fluorescent signals.

To directly read out PIFE effects in confocal single-molecule fluorescence microscopy, we utilized ALEX (Fig. S2A and Methods Section) for studies of fluorescently-labelled dsDNA.[8,41,57,58] Here, either Cy3 or Cy3B were combined with the FRET-acceptor ATTO647N. In ALEX histograms, the stoichiometry, S, allows to sort different molecular species according to their labelling: donor-only labelled dsDNA (S>0.8), acceptor-only labelled dsDNA (S<0.2) and donor-acceptor-labelled dsDNA 0.8>S>0.2 (Supplementary Fig. 2B). Since we are mostly interested in the properties of the species with both donor and acceptor labelling, we represent the final data set using a dual-colour burst search showing S over the proximity ratio $E_{PR}$. S at this stage is denoted $S(E_{PR})$ in Figure 3; the data was corrected for background and spectral cross talk[35] after an all-photon burst search.

At a separation of 40 bp between donor and acceptor fluorophores (>10 nm), the proximity ratio is zero due and forms a prominent population in the ALEX histogram at intermediate peak S-values of ~0.3 (Fig. 3A, Cy3). Values for $E_{PR}$ and $S(E_{PR})$ were derived from a two-dimensional global Gaussian fit (see Material and Methods) represented as a black circle at full-width-half-maximum (FWHM).

bioRxiv preprint doi: https://doi.org/10.1101/047779; this version posted May 11, 2016. The copyright holder for this preprint (which was not certified by peer review) is the author/funder. All rights reserved. No reuse allowed without permission.

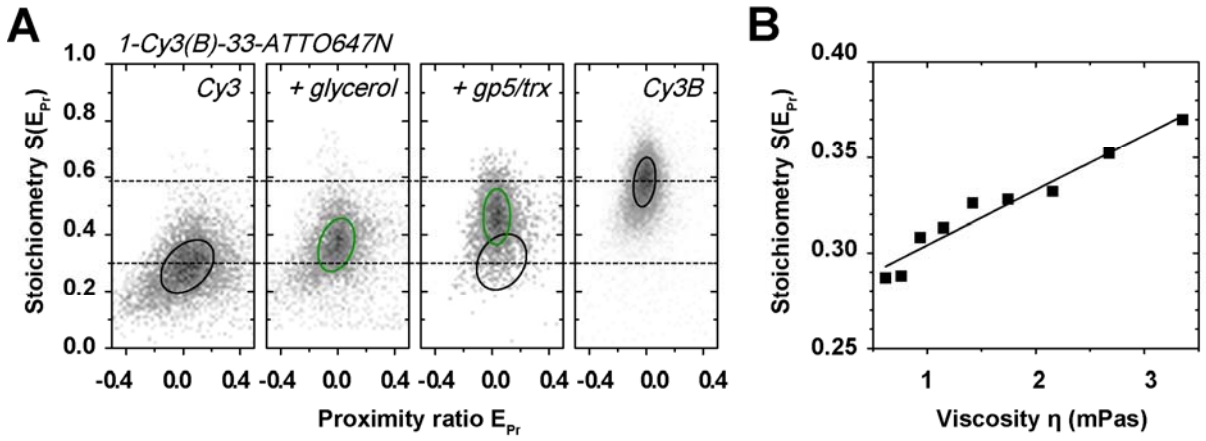


**Figure 3. Observing the PIFE effect in ALEX histograms. (A)** Cy3-ATTO647N, Cy3-ATTO647N with 40% glycerol, Cy3-ATTO647N in the presence of 30 nM T7 polymerase gp5/trx and Cy3B-ATTO647N. 2D Gaussian fitting was applied to characterize the observed populations; black/green circles mark the FWHM of each distribution in the presence (green) and absence (black) of brightness changes of the donor Cy3. **(B)** $S(E_{PR})$ as a function of viscosity[59] η using different concentrations of glycerol. The presented data is based on 45-mer dsDNA with large donor-acceptor separation of 33 bp (see Fig. S4A for oligonucleotide sequences and labelling positions). Relative differences of stoichiometry were found to be independent of laser power.

Addition of glycerol can emulate PIFE due to increase in bulk viscosity, which drives an increase in the mean fluorescence quantum yield of the Cy3 donor (Fig. 3A/S1F). As expected for such an increase, the donor-based photon streams DD and DA increase (data not shown), which hence increases $S(E_{PR})$ upon addition of glycerol to the imaging buffer (Fig. 3A, Cy3 + glycerol). We find a linear increase suggesting that the PIFE-effect can indeed serve as a molecular ruler (Fig. 3B). A similar effect, as for increasing viscosity through the addition of glycerol, is observed upon steric hindrance caused by non-specific binding of T7 polymerase gp5/trx[60-62] to dsDNA in close proximity to the Cy3 donor (Figure S3A). In Figure 3A a prominent PIFE population is seen at elevated $S(E_{PR})$-values when using concentrations of gp5/trx >50 nM (Figs. S3B/C). Similar PIFE-effects with a donor-enhanced QY, i.e., increase in $S(E_{PR})$, are found for Alexa Fluor 555 (Fig. S3D) or with acceptor-enhanced quantum yield for ATTO647N and Cy5 (Figs. S3E/F). The herein presented results indicate that PIFE-FRET provides the capability to binding of unlabeled protein.

In ALEX-based PIFE-FRET, ideally only one fluorophore should be influenced by protein binding while the other should have an constant fluorescence signal for normalization of the PIFE-sensitive signal. This is best fulfilled in case of a small protein

bioRxiv preprint doi: https://doi.org/10.1101/047779; this version posted May 11, 2016. The copyright holder for this preprint (which was not certified by peer review) is the author/funder. All rights reserved. No reuse allowed without permission.

footprint not allowing interaction with the acceptor or use of acceptor fluorophore that is micro-environment insensitive. In our hands, only TMR and Cy3B show little to no PIFE effect (Fig. S3) while Cy3, Alexa555, Cy5 and ATTO647N are all influenced by protein binding.

To determine the maximally achievable PIFE-effect for Cy3, we investigated the dsDNA labelled with Cy3B/ATTO647N and compared the S-value to Cy3/ATTO647N (Fig. 3A). The ~4.1-fold increase in brightness between Cy3 and Cy3B poses a practical upper limit as seen through the reported, maximal PIFE-effect of ~2.7-fold brightness increase for binding of the restriction enzyme *Bam*HI on dsDNA.[15-19] A comparison of $S(E_{PR})$ values between both samples hence emulates the maximal PIFE effect for ALEX experiments. In the absence of FRET, we find a range of $S(E_{PR})$ from 0.29 (Cy3) to 0.59 for Cy3B (Fig. 3A).

**Spatial sensitivity of the PIFE ruler in ALEX.** Next, we investigated the spatial sensitivity of the PIFE ruler (distance $R_1$) in ALEX experiments. By using a similar experimental scheme as introduced by Hwang et al.[16], we designed different dsDNAs with a sequence to accommodate specific binding of the restriction enzyme *Bam*HI (Fig. S5) at different $R_1$ distances from the donor Cy3(B) (Fig. 4A). The donor-acceptor $R_2$ distance was kept constant at 40 bp separation resulting in zero peak FRET efficiency (not to be mistaken with a donor-only species), while the binding site for the restriction enzyme was varied from 1,2,3,5 and up to 7 bp relative to the donor binding position (Fig. 4A). See Materials and Methods for the precise labelling scheme of the used dsDNAs. Restriction enzymes provide an excellent model system to study PIFE-FRET due to the well-characterized biochemical and structural behaviour[63-65]; both enzymes have been crystalized on dsDNA in the presence of calcium and bind as a homo-dimer (Fig. S5; pdb code: 2BAM). *Bam*HI forms a stable, pre-reactive complex on dsDNA containing the palindromic sequence GGATCC without changing the conformation of the dsDNA. In a modified assay, we explored *Eco*RV binding to a GATATC-site. In contrast to *Bam*HI, binding of *Eco*RV results in a tightly bound dsDNA conformation bent by 50°.

Figure 4B shows experimental data of *Bam*HI binding to different positions on DNA revealing the ruler-character of ALEX-based PIFE (Fig. 4B/S6). Upon addition of

bioRxiv preprint doi: https://doi.org/10.1101/047779; this version posted May 11, 2016. The copyright holder for this preprint (which was not certified by peer review) is the author/funder. All rights reserved. No reuse allowed without permission.

500 nM *Bam*HI [66], we observed two sub-populations in S: the isolated Cy3-containing DNA ($S(E_{PR})$ ~ 0.3) and a new PIFE-related population, i.e., *Bam*HI bound to DNA at higher $S(E_{PR})$ values (Fig. 4B). Optimal concentration for the *Bam*HI ruler was determined by monitoring PIFE with different *Bam*HI concentrations (Fig. S6); 1-Cy3-40-ATTO647N(1bp) showed a $K_d$ of ~ 40 nM. It should be noted, however, that the affinity between *Bam*HI and the respective DNA varies for different positions of the *Bam*HI binding site (see amplitudes of the PIFE-species in Figs. 4C/S6E). The control experiment of *Bam*HI binding in close proximity (1bp) to Cy3B shows a nearly unaltered peak stoichiometry upon binding to the dsDNA, which reports on a small decrease of Cy3B-intensity (Fig. S10A).

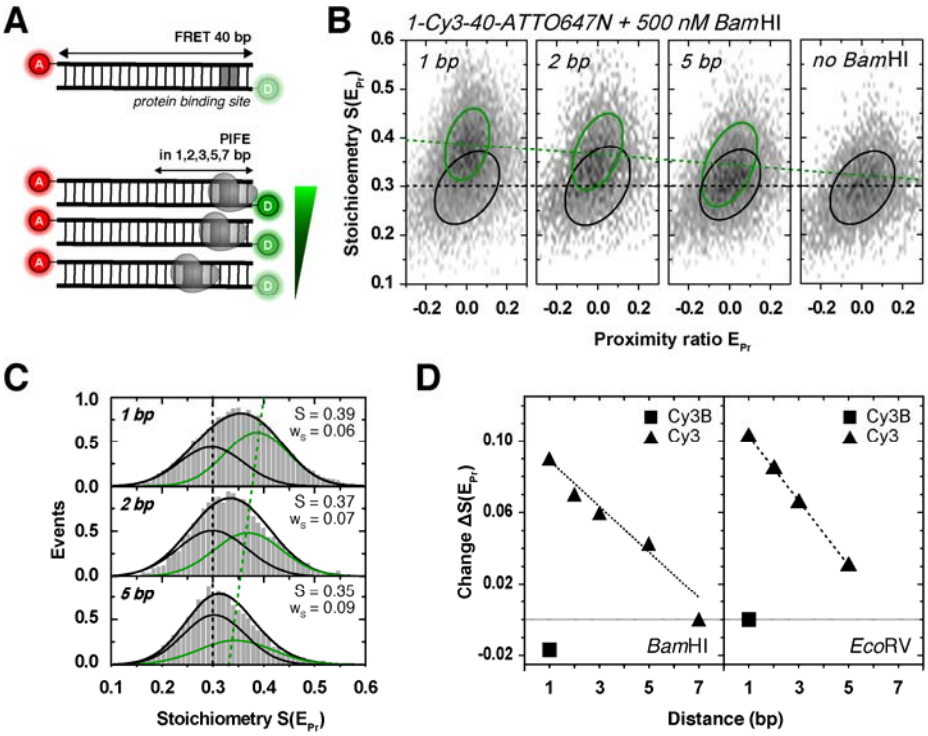


**Figure 4. The PIFE ruler in ALEX microscopy. (A)** Schematic of a dsDNA template containing a protein binding site of the restriction enzymes *Bam*HI and *Eco*RV positioned in $R_1$ = 1,2,3,5 and 7 bp distance from donor fluorophore Cy3. The acceptor ATTO647N is positioned at the opposite 5'-end in $R_2$ = 40 bp distance. **(B)** 2D histograms of 40 bp-dsDNA: free DNA (black circle) and DNA bound to 500 nM *Bam*HI with PIFE (green, circle) in 1,2 and 5 bp distance. 2D Gaussian fitting was applied to characterize the observed populations; black/green circles mark the FWHM of each distribution. **(C)** *Bam*HI-bound 40 bp-dsDNA: one dimensional projections of $S(E_{PR})$ data and 2D Gaussian fits and their centre positions (free form, black; protein-bound form, green). **(D)** Absolute changes in $S(E_{Pr})$ as function of $R_1$ between Cy3 and *Bam*HI (left) or *Eco*RV (right). Note that the control experiment with Cy3B (square) showed only little change of $S(E_{Pr})$ compared to Cy3 (triangle) even at close proximity of Cy3B and protein of 1 bp.

bioRxiv preprint doi: https://doi.org/10.1101/047779; this version posted May 11, 2016. The copyright holder for this preprint (which was not certified by peer review) is the author/funder. All rights reserved. No reuse allowed without permission.

The distance dependence of the PIFE-ruler is approximately linear with similar dependency as reported[16], i.e., 1-7 bp (Fig. 4D). The actual position of the Cy3 fluorophore (terminal vs. internal on the DNA) was found to have only a small influence on the observed S changes (Fig. S7). The absolute values of PIFE-readout S, however, differ for comparable laser powers between internal and terminal labelling. Hence the donor brightness and also the PIFE effect changes with the labelling position on DNA. This effect should be considered when designing PIFE-FRET assays. When performing identical experiments as for *Bam*HI (Fig. 4) with a different restriction enzyme (*Eco*RV, Fig. 4D/S8), we found a steeper distance dependence with an even more pronounced PIFE-effect. These results reveal the universal nature of the PIFE-ruler, but also that its specific quantitative properties require careful characterization for each biomolecular system – not only when used in PIFE-FRET but any other bulk or single-molecule assay.

**Calibration of the two rulers: $R_0$-correction for Cy3-PIFE in the presence of FRET.**

In the preceding section we have shown that the PIFE-ruler has a clear signature in ALEX experiments that renders it a useful tool for mechanistic biomolecular studies (Figs. 1C and 4). Since Cy3-PIFE is based on a competition of the radiative fluorescence transition $k_{D,T}$ and the (non-radiative) isomerizsation $k_{iso}$, its combination with FRET is complicated by the fact that energy transfer also depletes the donor excited state via $k_{FRET}$ (Fig. 2). S depends only on the donor-excitation based fluorescence intensities that are altered by PIFE when using an environmentally insensitive acceptor. Different peak E values can indicate (i) real distance changes between the donor and acceptor or (ii) changes in $R_0$ caused by altered donor QY for PIFE. A direct comparison of FRET efficiencies and related molecular distances for species with donor Cy3 and Cy3B with PIFE is impossible due to their different Förster radii $R_0$ – a situation that is similar to comparing the FRET efficiencies of donor-fluorophores Cy3 and Cy3B in combination with identical acceptor fluorophores. When comparing a DNA-based ladder of Cy3(B)/ATTO647N with $R_2$ separations of 8, 13, 18, 23, 28 and 33 bp (Fig. S4A), the problem becomes evident. We use corrected data $E_{PR}$

bioRxiv preprint doi: https://doi.org/10.1101/047779; this version posted May 11, 2016. The copyright holder for this preprint (which was not certified by peer review) is the author/funder. All rights reserved. No reuse allowed without permission.

/ $S(E_{PR})$ to read out brightness differences (Figs. 5A/D left panel; PIFE as an indicator distance $R_1$). A direct comparison of the S-shift indicative of PIFE decreases directly with increasing FRET (Fig. 5D) – indicating the competition between FRET and PIFE[67]. This data suggests that the dynamic range of the PIFE-FRET assay regarding distance $R_1$ (the range between S for Cy3 and for Cy3B, for a given E value) is optimal at low FRET efficiencies[67]. Accurate FRET values[35] are required to obtain distances on the FRET axis, i.e., distance $R_2$. A comparison of identical dsDNA having either Cy3 or Cy3B as a donor with 13 and 23 bp $R_2$ separations from the acceptor reveal significant differences in their peak accurate FRET E values (Fig. 5B). These differences of fluorophore pairs with identical interprobe distance reflect the shorter $R_0$ of Cy3-ATTO647N ($R_0$ = 5.1 nm[68]) as compared to Cy3B-ATTO647N ($R_0$ = 6.2 nm[69]).

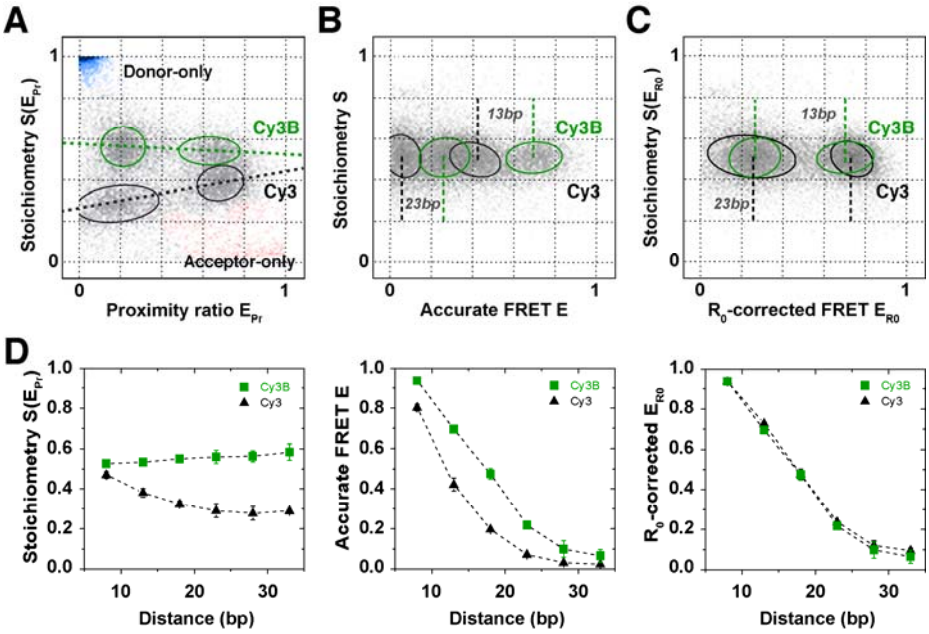


**Figure 5. Validation of the PIFE-FRET correction procedure in ALEX (A) Data correction process, to obtain $R_0$-corrected 2D-histograms.** Four dsDNAs with identical sequence (Fig. S4A) are labelled with two different FRET pairs: Cy3(B)/ATTO647N and mixed together. The donor is attached at the 5'-end; the difference in brightness between Cy3 (black) and Cy3B (green) separates the four populations into two groups according to $S(E_{Pr})$. The acceptor fluorophore ATTO647N is positioned on the complementary DNA strand in 13 and 23 bp distance; the two distances are deciphered via two different $E_{Pr}$ values per subgroup. (**B**) By correcting each fluorophore pair with its corresponding gamma factor $\gamma_{Cy3}$ or $\gamma_{Cy3B}$, accurate FRET values E for each population are obtained. The mean accurate FRET values for 13 or 23 bp differ between the two FRET-pairs due a difference in Förster radius $R_0$. (**C**) The proposed $R_0$-correction allows to convert all accurate FRET values on one common $R_0$-axis. **(D)** ALEX-data for 8, 13, 18, 23, 28 and 33 bp after the 3 correction steps, against background, gamma and $R_0$. Error bars were obtained from n = 4 experimental repeats.

bioRxiv preprint doi: https://doi.org/10.1101/047779; this version posted May 11, 2016. The copyright holder for this preprint (which was not certified by peer review) is the author/funder. All rights reserved. No reuse allowed without permission.

To allow a direct comparison of FRET efficiencies with and without PIFE, we suggest the following data analysis procedure (Fig. S2B). **Step 1:** raw data on the level of apparent FRET are corrected for background and spectral crosstalk[35] to retrieve the distance $R_1$ from PIFE (Fig. S2B). **Step 2:** By subsequent gamma correction, i.e., taking detection and quantum yield differences of donor and acceptor into account[35] accurate FRET values are obtained. Please note that Cy3 and Cy3-PIFE needs to be treated with a distinct gamma factor. **Step 3:** Finally, a correction for the differing $R_0$-values is needed that transforms the relevant FRET populations (Cy3, Cy3-PIFE, Cy3B) on the basis of the same $R_0$. For this we use Cy3B as a standard since the quantum yield of the latter is fixed and more or less independent of either the FRET efficiency or of the environment. Comparing two cases with and without PIFE assumes during PIFE only the donor QY, $\phi_D$, is altered (and not dye orientation or other factors) and hence approximate $R_0$ in the presence of PIFE as in equation 1:

$$R_0 \approx R_{0,ref}\left(\frac{\phi_D}{\phi_{D,ref}}\right)^{1/6} \qquad \textbf{(Eq. 1)}$$

Using the relation between accurate FRET E, interprobe distance *r* and $R_0$, we derive the $R_0$ corrected FRET efficiency $E_{R0}$ considering the $\ell$-fold enhancement of the donor-quantum-yield caused by PIFE. This enhancement factor can be obtained directly from the ratio of the two gamma-factors, which are proportional to the quantum yields of Cy3 and Cy3B, assuming constant detection efficiencies and negligible spectral shifts (equation 2):

$$E_{R0} = \frac{E}{\frac{1}{\ell}(1-E)+E} = \frac{E}{\frac{\gamma}{\gamma_{ref}}(1-E)+E} \qquad \textbf{(Eq. 2)}$$

We suggest the reference $\gamma_{ref}$ to be that of unbound Cy3B-labelled dsDNA. Using the definition of $E_{R0}$ as in Eq. 2, the FRET efficiency is decoupled from $R_0$ changes and related only to distance changes standardized to the $R_0$ value of free Cy3B on dsDNA (See Supplementary Note 1 for a complete derivation of equations 1 and 2 and Fig. S2 for a complete schematic overview of the data analysis).

bioRxiv preprint doi: https://doi.org/10.1101/047779; this version posted May 11, 2016. The copyright holder for this preprint (which was not certified by peer review) is the author/funder. All rights reserved. No reuse allowed without permission.

We tested this procedure by "aligning" the data sets of Cy3- and Cy3B-labelled DNA in combination with FRET acceptor ATTO647N. Using Eq. 2 we normalized the Cy3-data set to that of Cy3B by $R_0$-correction. As seen in Figure 5C for 13 and 23 bp and all other $R_2$ distances (Fig. 5D, right panel), $E_{RO}$ values of both fluorophore pairs are in excellent agreement validating our data analysis procedure. We note that equation 2 and the information given in Supplementary Note 1 provide a general possibility to account for changes in donor QY even by other photophysical processes such as quenching[68] (black-hole quencher etc.).

For use of PIFE-FRET in complex biochemical systems, i.e., where correction factors for individual populations may not be accessible, we suggest the use of a simplified data correction procedure. Here, the raw data on the level of apparent FRET are corrected for background and spectral crosstalk[35]. By subsequent gamma correction with the gamma value of Cy3B, we obtain accurate FRET values that are all normalized to the Cy3B-$R_0$-axis. This scheme is described in detail in Supplementary Note 2 (eqn. 6-11) and does not require determination of correction factors for individual populations. A comparison of Cy3- and Cy3B-labelled DNA with both analysis methods (see $R_0$-correction above) reveals that this method is a valid approximation (Figure S9), but the full correction procedure detailed in Figure 5 remains more accurate.

**PIFE-FRET monitors nucleic acid protein interactions and associated conformational changes.** The data in Figure 5 can only demonstrate the possibility to remove apparent changes in FRET efficiency caused by mere donor QY changes by an "$R_0$-correction". Next, we performed experiments where both PIFE and FRET are altered (and determined) within one experiment due to binding-associated conformational changes of dsDNA. For this we tested the signature of binding of *Bam*HI and *Eco*RV in PIFE-FRET at close proximity ($R_1$=1 bp) from the donor and at varying $R_2$ distances (Fig. 6A). Both restriction enzymes have different binding modes on DNA, i.e., *Bam*HI binding should not alter DNA conformation while *Eco*RV induces a 50° kink in the DNA after binding. Hence *Bam*HI is expected to show a PIFE effect but preserve FRET after binding, while *Eco*RV should show both PIFE and FRET signal changes.

bioRxiv preprint doi: https://doi.org/10.1101/047779; this version posted May 11, 2016. The copyright holder for this preprint (which was not certified by peer review) is the author/funder. All rights reserved. No reuse allowed without permission.

The ruler characteristics of PIFE and FRET, i.e., signal- to base-pair dependence for *Bam*HI, *Eco*RV and Cy3(B)-ATTO647N were described in Figures 4D and 5D.

In these experiments we use the full $R_0$-correction and a final normalization to Cy3B-gamma (Figure 6); the provided values of all measurements in Figure 6 can be compared directly. For *Bam*HI we expected no changes in the dsDNA conformation but a pronounced PIFE effect after binding (Fig. 6B); the experimentally observed PIFE effect is constant for all observed DNAs (Fig. 6C) and is consistent with the ruler distance for $R_1$ of 1 bp. PIFE effect is also only observed when using Cy3 as a donor fluorophore (Fig. 6C). Interestingly, the FRET ruler (distance $R_2$) shows a pronounced decrease of $E_{R_0}$ values after binding of *Bam*HI (Fig. 6B). Our data allows concluding that this observation is not an artefact of PIFE-FRET nor it is an artefact of our data analysis procedure, but rather a real increase of the donor-acceptor distance, since we observe similar trends when using Cy3B (Figs. 6C/S10), TMR or Atto550 as a donor (data for the latter two not shown).

bioRxiv preprint doi: https://doi.org/10.1101/047779; this version posted May 11, 2016. The copyright holder for this preprint (which was not certified by peer review) is the author/funder. All rights reserved. No reuse allowed without permission.

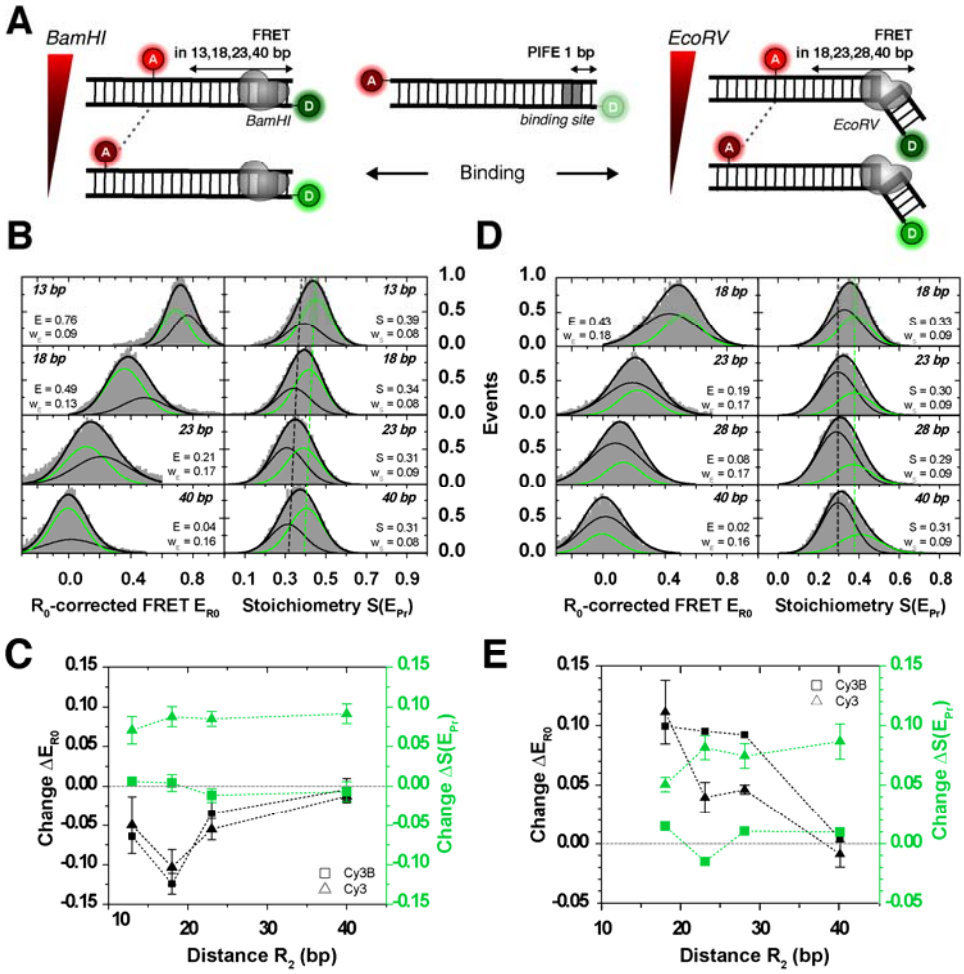


**Figure 6. Distance changes determined via FRET in the presence of PIFE.** FRET between Cy3/ATTO647N attached to a 40 bp-dsDNA is probed simultaneously to PIFE that occurred between Cy3 and different restriction enzymes in $R_1$ = 1 bp distance to the donor. **(A)** Schematic of DNA constructs probing FRET distances in 13, 18, 23 and 40 bp between ATTO647N and Cy3(B) in the presence of *Bam*HI, respectively in 18, 23, 28 and 40 bp in the presence of *Eco*RV. While *Bam*HI does not interfere with the 3D structure of the DNA, *Eco*RV is reported to introduce a 50° kink. **(B)** 1D ALEX histograms showing 500 nM *Bam*HI bound to 1bp-Cy3-*Bam*HI-dsDNA. Binding is detected as constant shift in S between ~ 0.3 (black) and ~ 0.4 (green). *Bam*HI introduces a conformational change in the dsDNA seen by smaller FRET values. **(C)** Differences in Stoichiometry $\Delta S(E_{Pr})$ and $R_0$-corrected FRET $\Delta E_{R0}$ between free and *Bam*HI-bound DNA. While binding is observed via PIFE of Cy3 (green, triangle), it is undetected for Cy3B (green, square). The conformational change in FRET is also observed for Cy3B (black, square). (**D**) 1D ALEX histograms showing 50 nM *Eco*RV bound to 1bp-Cy3-*Eco*RV-dsDNA. Binding is observed as a constant shift in S from 0.29 to 0.38. *Eco*RV is reported to kink dsDNA, which is observed by increased FRET values. **(E)** Differences in Stoichiometry $\Delta S(E_{Pr})$ and $R_0$-corrected FRET $\Delta E_{R0}$ between free and *Eco*RV-bound DNA labelled with Cy3 (triangle) or Cy3B (square). While distance changes in $R_2$ for different FRET distances are observed for both donor fluorophores (black panel), binding is only observed via PIFE to Cy3 (green, triangle) and undetected for Cy3B (green, square). Error bars were obtained from at least n = 2 experimental repeats. Full data sets and controls provided in Figure S10.

bioRxiv preprint doi: https://doi.org/10.1101/047779; this version posted May 11, 2016. The copyright holder for this preprint (which was not certified by peer review) is the author/funder. All rights reserved. No reuse allowed without permission.

The current understanding of *Bam*HI-interactions with dsDNA suggests that there should be only minor structural changes in dsDNA after binding[63]. We hence hypothesize that the FRET decrease (Figs. 6B/C) corresponds to a reduction of the accessible volume of Cy3(B) due to steric restriction of the dyes due to the space the protein occupies; such changes might be accompanied by changes of orientation factor $\kappa^2$. This interpretation is consistent with the fact that the decrease (and hence steric exclusion) is most pronounced when acceptor dye and protein are closer to each other. Such exclusion effects have to be considered especially when short-range interactions of DNA and proteins are measured by PIFE or other photophysical methods. Additional control experiments with the DNA-sliding T7 polymerase gpt/trx (gp5/trx[60-62], Figs. S3/11) that binds non-specifically to dsDNA confirms our data analysis procedure ($R_0$-correction, eqn. 1+2): T7 polymerase binding on dsDNA results in pronounced PIFE effects but constant $E_{R0}$ values (Fig. S11) verifying that the observed FRET changes for *Bam*HI binding are real and not caused by convolution of PIFE and FRET effects.

Performing similar experiments with *Eco*RV shows results that agree with structural predictions and reveal the full power of PIFE-FRET. A PIFE-effect consistent with 1 bp separation is found for all DNAs (Figs. 6D/E), which can only be observed for use of Cy3 as a donor fluorophore (Fig. 6E). As expected from the well-established kinking of *Eco*RV of dsDNA upon binding, the FRET ruler suggests a decrease in the donor-acceptor distance consistent upon binding and related DNA-kinking (Figs. 6D/E).

**PIFE-FRET maps initial transcription of E. coli RNA polymerase.** Finally, we used PIFE-FRET to study the *E. coli* RNA polymerase (RNAP) promoter DNA complex that still lacks full structural characterization due to its dynamic nature especially during transcription initiation. In an *in vitro* transcription assay of RNAP holoenzyme (core and $\sigma^{70}$ transcription factor) and lacCONS+20A model promoter, the enzyme melts and forms a ~13 bp DNA transcription bubble (registers -11 to +2) around the transcription start site at register +1 to form a transcription-competent RNAP-promoter open complex ($RP_O$). Subsequently, different subsets of nucleotide triphosphates (NTPs) were added in order to induce permanent abortive initiation pre-defined by the promoter sequence.[70] Through this procedure, different RNAP-promoter initially transcribed complex states

bioRxiv preprint doi: https://doi.org/10.1101/047779; this version posted May 11, 2016. The copyright holder for this preprint (which was not certified by peer review) is the author/funder. All rights reserved. No reuse allowed without permission.

($RP_{ITC\leq i}$, i – the maximal length of transcribed RNA, Figure S4E)[71,72] are visited at which the DNA bubble is scrunched by RNAP[73-75] allowing downstream DNA bases to melt and serve as reading template for polymerization of RNA.

To monitor the conformation of the DNA bubble in conjunction with its interaction with RNAP, we designed two PIFE-FRET assays with labelling of acceptor ATTO647N at -15 in the template (t) strand and the donor Cy3(B) at position +1/+3 at the nontemplate (nt) strand (Figure 7A). The ALEX data was analysed according to the simplified correction model outlined in Supplementary Note 2.

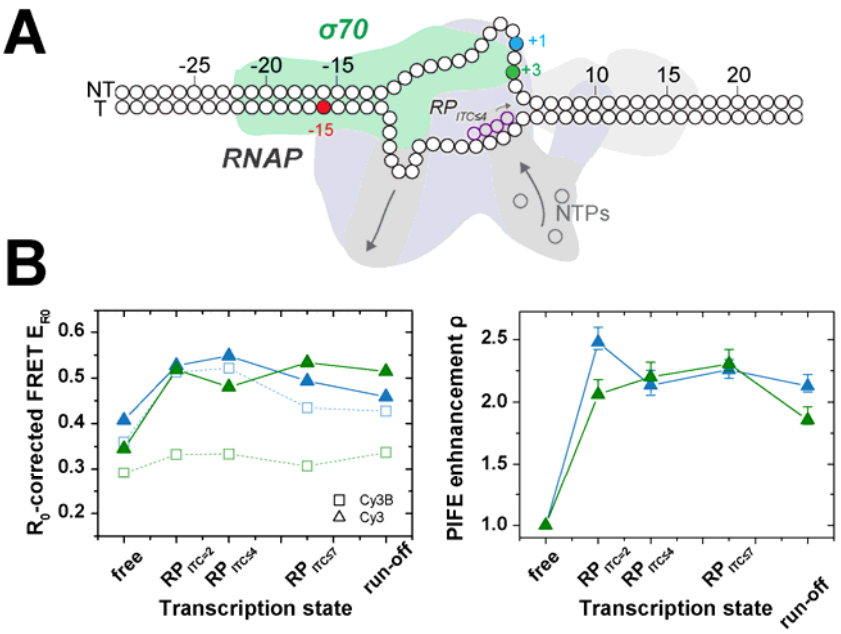


**Figure 7. Mapping the proximity of the scrunched transcription bubble with RNAP.** (**A**) Labelling scheme. The acceptor ATTO647N is positioned on the template strand at register (-15). The donor Cy3(B) is placed on the non-template strand at register (+1) (cyan) or (+3) (green). The dsDNA bound to the RNAP is depicted in an illustration of the transcription initiation state $RP_{ITC\leq 4}$ (**B**) Probing the scrunched transcription bubble for *RNA* transcription initiation in *E. Coli* using a lacCONS+20A dsDNA promoter[76,77] using PIFE-FRET. The $R_0$-corrected FRET values (left panel) and PIFE enhancement *ρ* (right panel) as provided for the registers -15/+1 (blue) and -15/+3(green). These results were achieved by a global fit of the data to the model provided by ref. 66 (see Fig. S12)..

For RNAP binding to promoter DNA, both +1/+3 donor *nt* registers report on bubble opening via a FRET increase from free DNA to $RP_{ITC=2}$. Scrunching is most pronounced in NTP-starved initiation states, $RP_{ITC\leq 4}$ and $RP_{ITC\leq 7}$ and having no full return of the bubble region to dsDNA in the run-off product shows RNAP is unable to run-off the labelled promoter sequence. These observations are in line with previous studies of

bioRxiv preprint doi: https://doi.org/10.1101/047779; this version posted May 11, 2016. The copyright holder for this preprint (which was not certified by peer review) is the author/funder. All rights reserved. No reuse allowed without permission.

initial transcription of E. coli RNAP. However, our data reveal the fine details of DNA scrunching when comparing how the bubble conformation changes when probes in reference to different *nt* registers. More specifically, register +1, which precedes register +3 in being part of the transcriptional bubble at an earlier initiation stage, shows an increase in FRET until reaching $RP_{ITC\leq4}$ then a decrease in FRET moving from $RP_{ITC\leq4}$ to $RP_{ITC\leq7}$, while register +3 seems to show this trend only starting at $RP_{ITC\leq7}$.

The PIFE readout shows S(E) values of free promoter DNA that change upon transition to initial transcribing complexes. In order to decouple PIFE increases in S from changes in S caused by an increase in E with no PIFE, the S(E) values were globally fitted to the model suggested in[67] (best fit results are shown as isolines in left panels). The absolute PIFE parameter values, which report on the fold-decrease in Cy3 cis/trans isomerization mobility, report on the complex changes in the proximity of the transcriptional bubble to RNAP most probably caused by scrunching. Interestingly Cy3 on *nt* register +1 shows a maximal PIFE effect in $RP_{ITC=2}$, then reduces upon scrunching in states $RP_{ITC\leq4}$ and $RP_{ITC\leq7}$. This reduction in the PIFE effect is accompanied by an increase in the PIFE effect for *nt* register +3 that is introduced to the bubble only after scrunching. (Figs. 7B/C). Regarding PIFE, the increase in peak stoichiometry for Cy3 is a first direct observation of RNAP binding in the vicinity of Cy3 close to position (+1/+3) of the *nt* strand.

These combined trends can possibly be interpreted as follows: during abortive initiation of transcription, the position of Cy3 in the *nt* strand as well as the structure of the DNA bubble vary relative to RNAP due to scrunching.. Lately Winkelman et al.[42] has shown how, in $RP_{ITC}$ states, *nt* registers (-2) - (+1) are extruded out of the surface of RNAP, by using cross-linking methods. The reduction in the PIFE with Cy3 labelling this specific position in the *nt* strand may indicate that this NTP-starved $RP_{ITC}$ state characterized by extrusion of the *nt* strand out of the RNAP surface exists also free in solution and is not only an outcome of possible cross-linking artefacts. In addition, these finding are strongly supported by the similar trends in the changes the conformation of the transcription bubble undergoes, as judged by FRET in reference to registers +1 and +3 in the *nt* strand.

bioRxiv preprint doi: https://doi.org/10.1101/047779; this version posted May 11, 2016. The copyright holder for this preprint (which was not certified by peer review) is the author/funder. All rights reserved. No reuse allowed without permission.

The effect observed through the FRET ruler can be interpreted as directly responding to the DNA scrunching, which shortens the distance between the downstream edge of the transcription bubble and bases upstream to it. However, how can the decrease in FRET efficiency in $RP_{ITC\leq7}$ be explained? Lerner and Chung have lately revealed the existence of a state in which transcription pauses for long periods of time and the nascent RNA backtracks by 1-2 bases into the secondary channel of RNAP in $RP_{ITC7}$.[70] One outcome is the decrease in bubble size and scrunching as confirmed by magnetic tweezer experiments.[70] Following the FRET results, a reduction in the bubble size can be inferred from the results using the *nt* register +1.[70] Although a reduction in the transcriptional bubble size and in scrunching is expected, how may it be different in the paused-backtracked state from the perspective of the bubble conformation? The simultaneous measurement of this effect through both FRET and PIFE offers an intriguing potential alternative route for the release of the strain built up by scrunching through the extrusion of the nontemplate strand out of the surface of RNAP.

Overall, these findings illustrate that PIFE-FRET allows probing of global conformational changes using FRET as well as changes in positioning of proteins along DNA, also in states where FRET changes are only subtle. The results shown here (Fig. 7) are the first report of a “dynamic footprint” of RNAP performing DNA scrunching in initiation. Scanning Cy3 attachment to all relevant template and nontemplate registers will yield a full picture of the “dynamic footprint” of RNAP bound to DNA in transcription initiation.

## DISCUSSION

To date there are a only few (single-molecule) assays allowing the simultaneous observation of both protein binding and the conformational changes associated with the binding event. One way is multi-colour ALEX which utilizes a FRET cascade of more than two fluorophore probes[36,78,79]. Although a powerful technique, it requires dye labelling of both nucleic acid and protein and sophisticated analysis that go even beyond the procedures introduced here.

bioRxiv preprint doi: https://doi.org/10.1101/047779; this version posted May 11, 2016. The copyright holder for this preprint (which was not certified by peer review) is the author/funder. All rights reserved. No reuse allowed without permission.

In this work, we realized a novel combination of protein-induced fluorescence enhancement (PIFE) and Förster resonance energy transfer (FRET). Our proposed technique allows for mechanistic investigations of protein-nucleic acid interactions with diffusion-based confocal microscopy or surface-immobilized molecules[80] without labelling of the protein of interest. This approach is compatible for single-molecule studies of weak (μM) interactions. After accounting for PIFE effects coupled to FRET, one can utilize PIFE-FRET to probe binding, global conformational changes in the Förster distance scales (3-10 nm) and local conformational changes on shorter distance scale (< 3 nm) and hence use the assay as a multi-scale quantitative ruler. Nevertheless, whereas the FRET dependence on distance between probes is well-established and general, the distance dependence of the PIFE effect requires careful characterization for each system under investigation, as it highly depends on the spatial topology of the binding surface, which brings about different steric hindrance effects for different binding modes of DNA with different proteins. In case of RNAP, we envision systematic experiments of RNAP e.g., free promoter DNA and $RP_O$ with the Cy3 dye labeling different registers on both the nontemplate and template strand, i.e., in the transcription bubble as well as at downstream positions. The results shown in Figure 7 re-affirm the existence of a DNA scrunching state[42], in which register +1 of the nontemplate strand is extruded out of the surface of RNAP in initially transcribing complex, while the transcription bubble size, enlarged by scrunching, decreases. This was found by use of PIFE-FRET without the use of chemical cross-linking agents. We therefore name these types of experiments by the name 'dynamic footprinting' and envision the technique will allow the characterization of dynamic conformational states, such as $RP_{ITC\leq i}$ states, that may be biased by the cross-linking procedure and are hard to capture using X-Ray crystallography.

As shown in Figure S3, the PIFE technique and also PIFE-FRET is not exclusive for cyanine fluorophores and Cy3 but other fluorescence quenching[68] (or enhancing) mechanisms can be used. An alternative mechanism is photo-induced electron transfer (PET) whereby Tryptophan or Guanosine may be used as specific fluorescence quenchers[81-83]. A FRET-PET hybrid technique has been recently introduced[84] and might, in principle, be coupled with PIFE. Nevertheless, this technique requires usage of

bioRxiv preprint doi: https://doi.org/10.1101/047779; this version posted May 11, 2016. The copyright holder for this preprint (which was not certified by peer review) is the author/funder. All rights reserved. No reuse allowed without permission.

specific fluorophores susceptible for PET by Trp, and also a Trp carrying protein with a well-characterized positioning for the PET to occur. With PIFE-sensitive fluorophores, the restriction of its steric freedom by a nearby bound protein alone is enough to induce the PIFE-effect. In addition, the dependence of the effect of PET on the dye-quencher distance is at the very short molecular separations which makes PET-relevant assays highly binary (ON/OFF), meaning that PET reports on a molecular contact distance and not more than that, while PIFE reports on distances up to 3 bp separation between dye and the surface of a bound protein, hence of more general applicability for probing complex biochemical processes.

To finally relate the distance dependencies of the PIFE-ruler present here to published smPIFE work, the fold increase in Cy3 fluorescence QY due to the PIFE effect is needed, which is only indirectly available in ALEX. In a forthcoming paper[67], we provide the needed photophysical framework for ALEX-based PIFE-FRET to demonstrate its ability to obtain fully quantitate experimental results from ALEX that are directly comparable with published smPIFE studies.

bioRxiv preprint doi: https://doi.org/10.1101/047779; this version posted May 11, 2016. The copyright holder for this preprint (which was not certified by peer review) is the author/funder. All rights reserved. No reuse allowed without permission.

## MATERIAL AND METHODS

**DNA, Proteins and Reagents.** Unless otherwise stated, reagents of luminescent grade were used as received. Amino-modified and fluorophore-labelled oligonucleotides were used as received (IBA, Germany). DNA single strands were annealed using the following protocol: A 5-50 µL of a 1 µM solution of two complementary single-stranded DNAs (ssDNA) was heated to 98 °C for 4 minutes and cooled down to 4 °C with a rate of 1 °C/min in annealing buffer (500 mM sodium chloride, 20 mM TRIS-HCl, and 1 mM EDTA at pH = 8).

Different sets of complementary DNA-oligonucleotides were used (Fig. S4). **Set 1**: The first scaffold uses two complementary 45-mers carrying the donors (Cy3, Cy3B, TMR or Alexa555) at the 5'-end of the top-strand (Fig. S4A). The acceptor (ATTO647N or Cy5) was attached in 8, 13, 18, 23, 28 or 33 bp separations to the donor fluorophore. The DNAs are referred to as e.g., 33bp-Cy3/ATTO647N for a sample with 33 bp separation between Cy3 on the top-strand and ATTO647N on the bottom-strand (Fig. S4A). Non-specific binding of T7 DNA polymerase gp5/thioredoxin via PIFE was investigated using 18/23/28/33bp-Cy3/ATTO647N as well as 33bp-(Cy3/Cy3b/AF555/TMR)/ATTO647N and 33bp-TMR/Cy5. T7 DNA polymerase gp5 was expressed and purified in a 1:1 complex with thioredoxin in E. Coli[85]. These samples were provided by the labs of van Oijen and Richardson.[85]. **Set 2**: To study the distance dependence of PIFE in absence of FRET we used DNAs comprising of 40-mers carrying Cy3(B) and ATTO647N (Fig. S4B). These DNAs separate both dyes by 40 bp which prohibits FRET-interactions due to large separation >10 nm. The DNAs carry palindromic sequences for two different restriction enzymes *Bam*HI and *Eco*RV at 1,2,3,5 and 7 bp distance with respect to Cy3(B) and are termed 1bp-Cy3(B)-*(#bp)*-*Bam*HI-40-ATTO647N for a dsDNA with 40 bp separation in FRET and *#bp* separation between the donor and *Bam*HI inducing PIFE. DNA sequences and positioning of *Bam*HI binding sites were adapted from ref.[16]; those for *Eco*RV were derived from 1bp-PIFE-*Bam*HI-DNA[16]. **Set 3**: To study the distance dependence of PIFE in presence of FRET, complementary 40-mer oligonucleotides carrying the donors (Cy3 and Cy3B) at the 5'-end of the top-strand and palindromic binding sequence for *Bam*HI and *Eco*RV in 1bp distance from the donor were employed (Fig. S4C). The acceptor (ATTO647N) was

bioRxiv preprint doi: https://doi.org/10.1101/047779; this version posted May 11, 2016. The copyright holder for this preprint (which was not certified by peer review) is the author/funder. All rights reserved. No reuse allowed without permission.

attached in 13,18,23 and 40 bp (*Bam*HI) respectively in 18,23,28 and 40 bp (*Eco*RV) distance to the donor fluorophore. The DNAs are termed (analogue to Set3) 1bp-Cy3(B)-1bp-*Bam*HI-(#bp)-ATTO647N for a dsDNA with 1bp separation in PIFE and *#bp* separation between the donor and the acceptor. DNA sequences and positioning for *Bam*HI and *Eco*RV were derived from 1bp-PIFE-*Bam*HI-DNA[16]. **Set 4:** To check the influence of internal and external labelling (Fig. S7) we attached Cy3 to the 3rd base pair in the top strand of 5bp-PIFE-*Bam*HI-DNA and ATTO647N at the 5'end of the bottom strand (Fig. S4D). We termed it 3bp-Cy3(B)-1bp-*Bam*HI-40-ATTO647N. *Bam*HI and *Eco*RV were used as received (NEB/Bioké, The Netherlands). **Set 5**: PIFE-FRET was employed to study the interaction between *E.Coli* RNA polymerase and promoter dsDNA during transcription initiation. In these experiments Oligos (Fig. S4E-F) having the lacCONS+20A sequence[77]. The template and nontemplate strands, were labeled with ATTO647N and Cy3(B) at different promoter registers as indicated in Figure S4 (IBA oligos, GmbH). RNAP holoenzyme was supplied by NEB, Ipswich, MA, USA, M0551S. High-purity ribonucleotide triphosphates (NTPs) (GE Healthcare, Little Chalfont, Buckinghamshire, UK) as well as Adenylyl(3′-5′) adenosine (ApA; Ribomed, Carlsbad, CA, USA) were used in all transcription reactions at 100 µM each.

ALEX-experiments were carried out at 25-50 pM of dsDNA at room temperature (22°C). For experiments on dsDNA only (Fig. S4A) or in combination with gp5/trx, an imaging buffer based on 50 mM TRIS-HCl, 200 mM potassium chloride at pH 7.4 was applied. 1 mM Trolox[86,87] and 10mM MEA were added to the buffer for photostabilization as reported in ref. [88]. Experiments with *Bam*HI were carried out in 50 mM TRIS-HCl, 100 mM sodium chloride, 10 mM CaCl2 and 0.1 mM EDTA at pH 7.4 in the presence of 143 mM bME. Experiments with *Eco*RV were carried out in 50 mM TRIS-HCl, 100 mM sodium chloride, 10mM CaCl2 and 0.1 mM EDTA at pH 7.4. All binding experiments with *Bam*HI and *Eco*RV were performed in the presence of calcium chloride, to prevent enzymatic activity[63-65] and the formation of aggregates[66].

**RNA polymerase transcription assays.** 10 µl of pre-solutions were prepared by 180 nM RNA Polymerase (RNAP) holoenzyme in TB buffer (50 mM Tris-HCl, pH 8, 100 mM KCl, 10 mM MgCl2, 1 mM DTT, 100 µg/ml BSA, and 5% glycerol). Solutions

bioRxiv preprint doi: https://doi.org/10.1101/047779; this version posted May 11, 2016. The copyright holder for this preprint (which was not certified by peer review) is the author/funder. All rights reserved. No reuse allowed without permission.

were incubated 20 min at 30°C, then 0.6µl of 1µM promoter DNA was added, and samples were further incubated 30 min at 37°C. 1 µl of 100 mg/ml Heparin-Sepharose suspension (GE Healthcare, Inc.) was added with 20 µl of KG7 buffer (40 mM HEPES-NaOH, pH 7, 10 mM $MgCl_2$, 1 mM DTT, 1 mM MEA, and 100 µg/ml BSA) ,then incubate 1 min at 37°C, to eliminate free RNAPs as well as RNAP binding promoter non-specifically. After 1 min incubation, samples were centrifuged using a table top centrifuge, and 15 µl of supernatants were transferred to tubes containing 15 µl of KG7 buffer incubate 30 min at 37°C to make $RP_O$ solutions. In order to make each transcription initial complexes, 4 µl of $RP_O$ solutions are transferred into 16 µl of solutions containing 0.625 mM $A_pA$ (for $RP_{ITC=2}$), 0.625 mM $A_pA$ + 0.625 mM UTP (for $RP_{ITC\leq4}$), 0.625 mM $A_pA$ + 0.625mM UTP + 0.625 mM GTP (for $RP_{ITC\leq7}$), 0.625 mM ATP + 0.625 mM UTP + 0.625 mM GTP (for $RD_{E=11}$)[77], or 0.625 mM of all NTPs (for Run-off)[77], in KG7 buffer, then incubate 30 min at 37°C.

**Fluorescence and anisotropy measurements.** Fluorescence spectra and anisotropy [89] values *R* were derived on a standard scanning spectrofluorometer (Jasco FP-8300; 20nm exc. and em. Bandwidth; 8 sec integration time) and calculated at the emission maxima of the fluorophores (for Cy3B, $\lambda_{ex}$ = 532 nm and $\lambda_{em}$ = 570 nm; for ATTO647N, $\lambda_{ex}$ = 640 nm and $\lambda_{em}$ = 660 nm), according to the relationship $R = (I_{VV} - GI_{VH})/(I_{VV} + 2GI_{VH})$. $I_{VV}$ and $I_{VH}$ describe the emission components relative to the vertical (V) or horizontal (H) orientation of the excitation and emission polarizer. The sensitivity of the spectrometer for different polarizations was corrected using horizontal excitation to obtain $G = I_{HV} / I_{HH}$. Steady-state anisotropy values for external Cy3 ($r_D$ = 0.231 ± 0.026), internal Cy3 ($r_D$ = 0.175 ± 0.036) and Cy3B ($r_D$ = 0.191 ± 0.007), and ATTO647 ($r_A$ = 0.110 ± 0.014), remained within the error range for all DNA constructs equal. In presence of *Bam*HI the anisotropy values slightly increase for external Cy3 ($r_D$ = 0.259 ± 0.033) and internal Cy3 ($r_D$ = 0.205 ± 0.044) and Cy3B ($r_D$ = 0.235 ± 0.032), and ATTO647N ($r_A$ = 0.149 ± 0.019). While both Cy3 and Cy3B show significantly high values to indicate stacking or groove binding[90], ATTO647N is freely rotating which guaranties that the FRET efficiency for all constructs is sensitive[58] to the inter-dye distance *r*.

bioRxiv preprint doi: https://doi.org/10.1101/047779; this version posted May 11, 2016. The copyright holder for this preprint (which was not certified by peer review) is the author/funder. All rights reserved. No reuse allowed without permission.

**Fluorescence lifetime measurements.** Fluorescence lifetimes were determined using time-correlated single-photon counting with a home-built confocal microscope described in ref.[91]. Fitting of the decay functions was done with a mono- (Cy3B, ATTO647N) or double-exponential function (Cy3) taking the instrumental response into account. Values reported in this section and Table 1 are given with an error of 5%. The data was processed via a custom data evaluation program[92] written in MATLAB (2013b, MathWorks Inc., Natick, MA). The procedure yielded a bi-exponential decay of 1.6 and 0.4 ns for Cy3, and mono-exponential decays of 2.29 ns for Cy3B and 4.24 ns for ATTO647N on a 40-mer dsDNA. The presence of *Bam*HI alters the lifetimes to 1.75 ns and 0.4 ns on average (Cy3), 2.22 ns (Cy3B) and 4.29 ns (ATTO647N). On a 45-mer DNA lifetimes of Cy3 (1.18 ns, bi-exponential average), Cy3B (2.30 ns), TMR (3.23 ns), Alexa555 (1.64 ns), ATTO647N (4.17 ns) and Cy5 (1.38 ns) were determined. Addition and non-specific binding of gp5/trx alters their lifetimes as follows: Cy3 (1.69 ns, bi-exponential average), Cy3B (2.5 ns), TMR (2.98 ns), ATTO647N (4.23 ns) and Cy5 (1.70 ns).

**ALEX-Spectroscopy and data analysis.** For single-molecule experiments custom-built confocal microscopes for µs-ALEX described in[93-95] were used as schematically shown in Figure S2. Shortly, the alternation period was set to 50 µs, and the excitation intensity to 60 µW at 532 nm and 25 µW at 640 nm. A 60x objective with NA=1.35 (Olympus, UPLSAPO 60XO) was used. Laser excitation was focused to a diffraction limited spot 20 µm into the solution. Fluorescence emission was collected, filtered against background (using a 50-µm pinhole and bandpass filters) and detected with two avalanche photodiode detectors (τ-spad, Picoquant, Germany). After data acquisition, fluorescence photons arriving at the two detection channels (donor detection channel: $D_{em}$; acceptor detection channel: $A_{em}$) were assigned to either donor- or acceptor-based excitation on their photon arrival time as described previously.[41,57] From this, three photon streams were extracted from the data corresponding to donor-based donor

bioRxiv preprint doi: https://doi.org/10.1101/047779; this version posted May 11, 2016. The copyright holder for this preprint (which was not certified by peer review) is the author/funder. All rights reserved. No reuse allowed without permission.

emission F(DD), donor-based acceptor emission F(DA) and acceptor-based acceptor emission F(AA; Fig. S2A).

During diffusion (Fig. S2B), fluorophore stoichiometries S and apparent FRET efficiencies E* were calculated for each fluorescent burst above a certain threshold yielding a two-dimensional histogram.[41,57] Uncorrected FRET efficiency E* monitors the proximity between the two fluorophores and is calculated according to:

$$E^* = \frac{F(DA)}{F(DD) + F(DA)} \qquad \textbf{(Eq. 3)}$$

S is defined as the ratio between the overall green fluorescence intensity over the stotal green and red fluorescence intensity and describes the ratio of donor-to-acceptor fluorophores in the sample S:

$$S = \frac{F(DD) + F(DA)}{F(DD) + F(DA) + F(AA)} \qquad \textbf{(Eq. 4)}$$

Using published procedures to identify bursts corresponding to single molecules[96], we obtained bursts characterized by three parameters (M, T, and L). A fluorescent signal is considered a burst provided it meets the following criteria: a total of L photons, having M neighbouring photons within a time interval of T microseconds. For all data presented in this study, a dual colour burst search[96,97] using parameters M = 15, T = 500 µs and L = 25 was applied; additional thresholding removed spurious changes in fluorescence intensity and selected for intense single-molecule bursts (all photons > 100 photons unless otherwise mentioned). Binning the detected bursts into a 2D E*/S histogram where sub-populations are separated according to their S-values. E*- and S-distributions were fitted using a Gaussian function, yielding the mean values $\mu_i$ of the distribution and an associated standard deviations $w_i$. Experimental values for E* and S were corrected for background, spectral crosstalk (proximity ratio $E_{PR}$) and gamma factor resulting in histograms of accurate FRET E and corrected S according to published procedures[35].

**Data analysis to retrieve distance $R_1$ (PIFE-ruler).** All data were corrected against background and spectral crosstalk to yield $E_{PR}$ and S($E_{PR}$). To determine the induced enhancement introduced by the change in Cy3 cis/trans isomerization monility either by

bioRxiv preprint doi: https://doi.org/10.1101/047779; this version posted May 11, 2016. The copyright holder for this preprint (which was not certified by peer review) is the author/funder. All rights reserved. No reuse allowed without permission.

viscosity (glycerol; Fig. 3) or by steric hindrance (caused by a binding protein close-by), the mean value of stoichiometry $S(E_{Pr})$ of the free DNA was determined via 2D-Gaussian fitting of the 2D $E_{Pr}$-$S(E_{Pr})$-histogram. DNA in the presence of a DNA-binding protein was fitted with two independent 2D Gaussian population, where one population – the unbound species – was approximated with constant values obtained for the free DNA species before. The observed PIFE enhancement was represented as difference in Stoichiometry $S(E_{Pr})$. The PIFE enhancement factor ρ that reports on the PIFE effect decoupled from S changes caused by pure E changes (without PIFE) was retrieved from an advanced model as described in ref.[67]. In brief, this model allows for the retrieval of the amount by which the excited-state *trans*/*cis* isomerization of Cy3 is slowed down (the fold decrease in *cis*/*trans* isomerization mobility).

**Data analysis to retrieve distance $R_2$ (FRET-ruler) in the presence of PIFE.** All data was corrected against background and spectral crosstalk. At ***first*** the $\gamma_{Cy3(B)}$ for all free DNAs was determined and free DNA's data was corrected until accurate FRET E. For this, all data needs to be corrected against background and spectral crosstalk. For both FRET pairs the individual gamma factors, $\gamma_{Cy3(B)}$ were determined, and each population was corrected with it obtaining accurate FRET E. In a ***second*** step, the gamma factor for the protein bound species $\gamma_{Cy3(B)/protein}$ is determined, and each population within the data set is corrected with its own individual $\gamma_{Cy3(B)/protein}$ and $\gamma_{Cy3(B)/free}$. This is achieved by assigning each burst of the uncorrected data at the beginning to either the free or bound DNA subpopulation (see next paragraph). This is followed by a selective accurate FRET correction for each subpopulation. After this correction step all determined $R_0$-corrected FRET values for the free and bound Cy3-dsDNA are converted onto the $R_0$-axis of the environmentally insensitive Cy3B by applying Eq. 2 burst-wise. The mean $R_0$-corrected FRET value $E_{R0}$ is determined by 2D-Gaussian fitting of the $E_{R0}$-S-histogram. FRET values of converted-Cy3 and Cy3B should be identical within errors at this correction stage. As convention, we transformed all presented $R_0$-corrected FRET values onto the unaltered $R_0$-axis of the free Cy3B-labeled DNA in this manuscript.

bioRxiv preprint doi: https://doi.org/10.1101/047779; this version posted May 11, 2016. The copyright holder for this preprint (which was not certified by peer review) is the author/funder. All rights reserved. No reuse allowed without permission.

**Population assignment.** In order to correct individual populations with different correction factors, as gamma factors, within one 2D ALEX histogram, every burst needs to be assigned to a particular population. This can be achieved via cluster analysis methods or probability distribution analysis[98]. In our implementation, every population in the uncorrected 2D histogram is first fitted with a covariant bivariate Gaussian function

$$f_i(E,S) = A\, exp\left\{-\frac{1}{2(1-\rho^2)}\cdot\left[\left(\frac{E-\mu_E}{w_E}\right)^2 - 2\rho\cdot\left(\frac{E-\mu_E}{w_E}\right)\cdot\left(\frac{S-\mu_S}{w_S}\right) + \left(\frac{S-\mu_S}{w_S}\right)^2\right]\right\} \qquad \textbf{(Eq. 5)}$$

where the population is described by an amplitude *A*, its mean values $\mu_i$ and standard deviations $w_i$ in FRET E* and Stoichiometry S. $\rho$ denotes the correlation matrix between E* and S. We express the probability $p$ that a given burst in the 2D histogram belongs to population $i$ by

$$p_i(E,S) = \frac{f_i(E,S)}{\sum_{j=1}^{n} f_j(E,S)} \qquad \textbf{(Eq. 6)}$$

For every bin in the 2D histogram, the algorithm calculates the number of bursts $n_i$ belonging to population $i$ by $n_i = n \cdot p_i(E,S)$, where $n$ is the number of burst in one bin. E and S are taken to be the bin centre. The corresponding bursts are assigned to a particular population $i$ and kept through out the data analysis process.

bioRxiv preprint doi: https://doi.org/10.1101/047779; this version posted May 11, 2016. The copyright holder for this preprint (which was not certified by peer review) is the author/funder. All rights reserved. No reuse allowed without permission.

## AUTHOR CONTRIBUTIONS

T.C. conceived the study. E.P., E.L., S.W., J.H. and T.C designed research. E.P., E.L., F.H., and S.C. performed research. E.L., J.H. and M.R. provided new analytical tools. E.P., E.L., M.R. and T.C. analysed data. The manuscript was written through contributions of all authors. All authors have given approval to the final version of the manuscript.

## FUNDING SOURCES

This work was financed by the Zernike Institute for Advanced Materials, the Centre for Synthetic Biology (Start-up grant to T.C.), an ERC Starting Grant (ERC-STG 638536 – SM-IMPORT to T.C.) as well as NIH (GM069709 to S.W.) and NSF (MCB-1244175 to S.W.), a Marie Curie Career Integration Grant (#630992 to J. H.). E.P. acknowledges a DFG fellowship (PL696/2-1).

## NOTES

The authors declare no competing financial interests.

## ACKNOWLEDGMENT

The authors are grateful to A.M. van Oijen for generous and enduring support including thoughtful discussions and advise. We thank A.M. van Oijen and C. Richardson for the kind gift of T7 DNA polymerase 5 (gp5/trx), G. Gkouridis and M.J. de Boer for fruitful discussions and advise.

bioRxiv preprint doi: https://doi.org/10.1101/047779; this version posted May 11, 2016. The copyright holder for this preprint (which was not certified by peer review) is the author/funder. All rights reserved. No reuse allowed without permission.

## REFERENCES


1. Kalinin, S. et al. A toolkit and benchmark study for FRET-restrained high-precision structural modeling. *Nature Methods* **9**, 1218-U129 (2012).
2. Muschielok, A. et al. A nano-positioning system for macromolecular structural analysis. *Nat Methods* **5**, 965-71 (2008).
3. McKinney, S.A., Declais, A.C., Lilley, D.M. & Ha, T. Structural dynamics of individual Holliday junctions. *Nat Struct Biol* **10**, 93-7 (2003).
4. Hyeon, C., Lee, J., Yoon, J., Hohng, S. & ThirumalaiD. Hidden complexity in the isomerization dynamics of Holliday junctions. *Nat Chem* **4**, 907-914 (2012).
5. Weiss, S. Fluorescence spectroscopy of single biomolecules. *Science* **283**, 1676-83. (1999).
6. Ha, T. Single-Molecule Fluorescence Resonance Energy Transfer. *Methods* **25**, 78-86 (2001).
7. Roy, R., Hohng, S. & Ha, T. A practical guide to single-molecule FRET. *Nat Methods* **5**, 507-16 (2008).
8. Hohlbein, J., Craggs, T.D. & Cordes, T. Alternating-laser excitation: single-molecule FRET and beyond. *Chem Soc Rev* **online**(2013).
9. Hohlbein, J., Gryte, K., Heilemann, M. & Kapanidis, A.N. Surfing on a new wave of single-molecule fluorescence methods. *Phys. Biol.* **7**, 031001 (2010).
10. Farooq, S., Fijen, C. & Hohlbein, J. Studying DNA-protein interactions with single-molecule Förster resonance energy transfer. *Protoplasma*, 1-16 (2013).
11. Yang, H. et al. Protein Conformational Dynamics Probed by Single-Molecule Electron Transfer. *Science* **302**, 262-266 (2003).
12. Chattopadhyay, K., Elson, E.L. & Frieden, C. The kinetics of conformational fluctuations in an unfolded protein measured by fluorescence methods. *Proceedings of the National Academy of Sciences of the United States of America* **102**, 2385-2389 (2005).
13. Bollmann, S. et al. Conformational Flexibility of Glycosylated Peptides. *Chemphyschem* **12**, 2907-2911 (2011).
14. Zhou, R.B., Kunzelmann, S., Webb, M.R. & Ha, T. Detecting Intramolecular Conformational Dynamics of Single Molecules in Short Distance Range with Subnanometer Sensitivity. *Nano Letters* **11**, 5482-5488 (2011).
15. Myong, S., Bruno, M.M., Pyle, A.M. & Ha, T. Spring-loaded mechanism of DNA unwinding by hepatitis C virus NS3 helicase. *Science* **317**, 513-516 (2007).
16. Hwang, H., Kim, H. & Myong, S. Protein induced fluorescence enhancement as a single molecule assay with short distance sensitivity. *Proceedings of the National Academy of Sciences of the United States of America* **108**, 7414-7418 (2011).
17. Luo, G., Wang, M., Konigsberg, W.H. & Xie, X.S. Single-molecule and ensemble fluorescence assays for a functionally important conformational change in T7 DNA polymerase. *Proc Natl Acad Sci U S A* **104**, 12610-5 (2007).
18. Hwang, H. & Myong, S. Protein induced fluorescence enhancement (PIFE) for probing protein-nucleic acid interactions. *Chem Soc Rev* (2013).
19. Vrtis, K.B., Markiewicz, R.P., Romano, L.J. & Rueda, D. Carcinogenic adducts induce distinct DNA polymerase binding orientations. *Nucleic Acids Res* **41**, 7843-53 (2013).
20. Kim, J.Y., Kim, C. & Lee, N.K. Real-time submillisecond single-molecule FRET dynamics of freely diffusing molecules with liposome tethering. *Nat Commun* **6**, 6992 (2015).
21. Torella, J.P., Holden, S.J., Santoso, Y., Hohlbein, J. & Kapanidis, A.N. Identifying Molecular Dynamics in Single-Molecule FRET Experiments with Burst Variance Analysis. *Biophysical journal* **100**, 1568-1577 (2011).
22. Tomov, T.E. et al. Disentangling subpopulations in single-molecule FRET and ALEX experiments with photon distribution analysis. *Biophys J* **102**, 1163-73 (2012).

bioRxiv preprint doi: https://doi.org/10.1101/047779; this version posted May 11, 2016. The copyright holder for this preprint (which was not certified by peer review) is the author/funder. All rights reserved. No reuse allowed without permission.


23. Gopich, I.V. & Szabo, A. Single-molecule FRET with diffusion and conformational dynamics. *J Phys Chem B* **111**, 12925-32 (2007).
24. Gopich, I.V. & Szabo, A. Decoding the Pattern of Photon Colors in Single-Molecule FRET. *The Journal of Physical Chemistry B* **113**, 10965-10973 (2009).
25. Kalinin, S., Valeri, A., Antonik, M., Felekyan, S. & Seidel, C.A.M. Detection of Structural Dynamics by FRET: A Photon Distribution and Fluorescence Lifetime Analysis of Systems with Multiple States. *The Journal of Physical Chemistry B* **114**, 7983-7995 (2010).
26. Hoffmann, A. et al. Quantifying heterogeneity and conformational dynamics from single molecule FRET of diffusing molecules: recurrence analysis of single particles (RASP). *Phys Chem Chem Phys* **13**, 1857-71 (2011).
27. Kapanidis, A.N. et al. Initial transcription by RNA polymerase proceeds through a DNA-scrunching mechanism. *Science* **314**, 1144-1147 (2006).
28. Robb, N.C. et al. The Transcription Bubble of the RNA Polymerase-Promoter Open Complex Exhibits Conformational Heterogeneity and Millisecond-Scale Dynamics: Implications for Transcription Start-Site Selection. *J Mol Biol* **425**, 875-885 (2013).
29. Crawford, R. et al. Long-Lived Intracellular Single-Molecule Fluorescence Using Electroporated Molecules. *Biophysical journal* **105**, 2439-2450 (2013).
30. Konig, I. et al. Single-molecule spectroscopy of protein conformational dynamics in live eukaryotic cells. *Nat Methods* **12**, 773-9 (2015).
31. Henzler-Wildman, K.A. et al. Intrinsic motions along an enzymatic reaction trajectory. *Nature* **450**, 838-44 (2007).
32. Person, B., Stein, I.H., Steinhauer, C., Vogelsang, J. & Tinnefeld, P. Correlated Movement and Bending of Nucleic Acid Structures Visualized by Multicolor Single-Molecule Spectroscopy. *Chemphyschem* **10**, 1455-1460 (2009).
33. Dean, K.M. & Palmer, A.E. Advances in fluorescence labeling strategies for dynamic cellular imaging. *Nat Chem Biol* **10**, 512-523 (2014).
34. Uphoff, S. et al. Monitoring multiple distances within a single molecule using switchable FRET. *Nature Methods* **7**, 831-836 (2010).
35. Lee, N.K. et al. Accurate FRET measurements within single diffusing biomolecules using alternating-laser excitation. *Biophys J* **88**, 2939-53 (2005).
36. Yim, S.W. et al. Four-color alternating-laser excitation single-molecule fluorescence spectroscopy for next-generation biodetection assays. *Clin Chem* **58**, 707-16 (2012).
37. Cohen, A.E. & Moerner, W.E. Controlling Brownian motion of single protein molecules and single fluorophores in aqueous buffer. *Opt Express* **16**, 6941-56 (2008).
38. Cohen, A.E. & Moerner, W.E. Suppressing Brownian motion of individual biomolecules in solution. *Proc Natl Acad Sci U S A* **103**, 4362-5 (2006).
39. Berglund, A. & Mabuchi, H. Tracking-FCS: Fluorescence correlation spectroscopy of individual particles. *Opt Express* **13**, 8069-82 (2005).
40. Tyagi, S. et al. Continuous throughput and long-term observation of single-molecule FRET without immobilization. *Nat Methods* **11**, 297-300 (2014).
41. Kapanidis, A.N. et al. Alternating-laser excitation of single molecules. *Acc Chem Res* **38**, 523-33 (2005).
42. Winkelman, J.T. et al. Crosslink Mapping at Amino Acid-Base Resolution Reveals the Path of Scrunched DNA in Initial Transcribing Complexes. *Mol Cell* **59**, 768-80 (2015).
43. Hwang, H., Kim, H. & Myong, S. Protein induced fluorescence enhancement as a single molecule assay with short distance sensitivity. *Proc Natl Acad Sci U S A* **108**, 7414-8 (2011).
44. Hwang, H. & Myong, S. Protein induced fluorescence enhancement (PIFE) for probing protein-nucleic acid interactions. *Chem Soc Rev* **43**, 1221-9 (2014).

bioRxiv preprint doi: https://doi.org/10.1101/047779; this version posted May 11, 2016. The copyright holder for this preprint (which was not certified by peer review) is the author/funder. All rights reserved. No reuse allowed without permission.

45. Kretschy, N. & Somoza, M.M. Comparison of the Sequence-Dependent Fluorescence of the Cyanine Dyes Cy3, Cy5, DyLight DY547 and DyLight DY647 on Single-Stranded DNA. *PLoS ONE* **9**, e85605 (2014).
46. Levitus, M. & Ranjit, S. Cyanine dyes in biophysical research: the photophysics of polymethine fluorescent dyes in biomolecular environments. *Quarterly Reviews of Biophysics* **44**, 123-151 (2011).
47. Rasnik, I., Myong, S., Cheng, W., Lohman, T.M. & Ha, T. DNA-binding orientation and domain conformation of the E. coli rep helicase monomer bound to a partial duplex junction: single-molecule studies of fluorescently labeled enzymes. *J Mol Biol* **336**, 395-408 (2004).
48. Sanborn, M.E., Connolly, B.K., Gurunathan, K. & Levitus, M. Fluorescence properties and photophysics of the sulfoindocyanine Cy3 linked covalently to DNA. *Journal of Physical Chemistry B* **111**, 11064-11074 (2007).
49. Gatzogiannis, E. et al. Mapping protein-specific micro-environments in live cells by fluorescence lifetime imaging of a hybrid genetic-chemical molecular rotor tag. *Chem Commun (Camb)* **48**, 8694-6 (2012).
50. Thompson, A.J., Tang, T.-Y.D., Herling, T.W., Hak, R.C., Mann, S., Knowles, T.P.J., Kuimova, M.K. Quantitative sensing of microviscosity in protocells and amyloid materials using fluorescence lifetime imaging of molecular rotors. *SPIE* **8947**(2014).
51. Stennett, E.M.S., Ciuba, M.A., Lin, S. & Levitus, M. Demystifying PIFE: The Photophysics Behind the Protein-Induced Fluorescence Enhancement Phenomenon in Cy3. *The Journal of Physical Chemistry Letters* **6**, 1819-1823 (2015).
52. Medina, M.A. & Schwille, P. Fluorescence correlation spectroscopy for the detection and study of single molecules in biology. *Bioessays* **24**, 758-64 (2002).
53. Jia, K. et al. Characterization of photoinduced isomerization and intersystem crossing of the cyanine dye Cy3. *J Phys Chem A* **111**, 1593-7 (2007).
54. Aramendia, P.F., Negri, R.M. & Roman, E.S. Temperature Dependence of Fluorescence and Photoisomerization in Symmetric Carbocyanines.Influence of Medium Viscosity and Molecular Structure. *The Journal of Physical Chemistry* **98**, 3165-3173 (1994).
55. Cooper, M. et al. Cy3B (TM): Improving the performance of cyanine dyes. *Journal of Fluorescence* **14**, 145-150 (2004).
56. Eftink, M.R., Selvidge, L. A. . Fluorescence quenching of liver alcohol dehydrogenase by acrylamide. *Biochemistry* **21**, 117-125 (1982).
57. Kapanidis, A.N. et al. Fluorescence-aided molecule sorting: analysis of structure and interactions by alternating-laser excitation of single molecules. *Proc Natl Acad Sci U S A* **101**, 8936-41 (2004).
58. Cordes, T. et al. Sensing DNA Opening in Transcription Using Quenchable Forster Resonance Energy Transfer. *Biochemistry* **49**, 9171-9180 (2010).
59. Cerimovic, S. et al. Sensing viscosity and density of glycerol–water mixtures utilizing a suspended plate MEMS resonator. *Microsystem Technologies* **18**, 1045-1056 (2012).
60. Etson, C.M., Hamdan, S.M., Richardson, C.C. & van Oijen, A.M. Thioredoxin suppresses microscopic hopping of T7 DNA polymerase on duplex DNA. *Proc Natl Acad Sci U S A* **107**, 1900-5 (2010).
61. Akabayov, B. et al. Conformational dynamics of bacteriophage T7 DNA polymerase and its processivity factor, Escherichia coli thioredoxin. *Proceedings of the National Academy of Sciences* **107**, 15033-15038 (2010).
62. Brieba, L.G. et al. Structural basis for the dual coding potential of 8-oxoguanosine by a high-fidelity DNA polymerase. *Embo j* **23**, 3452-61 (2004).
63. Viadiu, H. & Aggarwal, A.K. The role of metals in catalysis by the restriction endonuclease BamHI. *Nat Struct Biol* **5**, 910-6 (1998).

bioRxiv preprint doi: https://doi.org/10.1101/047779; this version posted May 11, 2016. The copyright holder for this preprint (which was not certified by peer review) is the author/funder. All rights reserved. No reuse allowed without permission.


64. Vipond, I.B., Baldwin, G.S. & Halford, S.E. Divalent Metal Ions at the Active Sites of the EcoRV and EcoRI Restriction Endonucleases. *Biochemistry* **34**, 697-704 (1995).
65. Kostrewa, D. & Winkler, F.K. Mg2+ binding to the active site of EcoRV endonuclease: a crystallographic study of complexes with substrate and product DNA at 2 A resolution. *Biochemistry* **34**, 683-96 (1995).
66. Engler, L.E. et al. The energetics of the interaction of BamHI endonuclease with its recognition site GGATCC. *Journal of Molecular Biology* **307**, 619-636 (2001).
67. Lerner, E., Ploetz, E., Hohlbein, J., Cordes, T. & Weiss, S. A theoretical framework for PIFE-FRET. *J Phys Chem B* **(submitted)**(2016).
68. Le Reste, L., Hohlbein, J., Gryte, K. & Kapanidis, A.N. Characterization of dark quencher chromophores as nonfluorescent acceptors for single-molecule FRET. *Biophys J* **102**, 2658-68 (2012).
69. Holden, S.J. et al. Defining the Limits of Single-Molecule FRET Resolution in TIRF Microscopy. *Biophysical Journal* **99**, 3102-3111 (2010).
70. Lerner, E. et al. A Novel Initiation Pathway in Escherichia Coli Transcription. *bioRxiv* (2016).
71. Smagowicz, W.J. & Scheit, K.H. Primed abortive initiation of RNA synthesis by E. coli RNA polymerase on T7 DNA. Steady state kinetic studies. *Nucleic Acids Res* **5**, 1919-32 (1978).
72. Munson, M.M., Reznikoff, W.S. Abortive initiation and long RNA synthesis. *Biochemistry* **20**, 2081-2085 (1981).
73. Kapanidis, A.N. et al. Initial transcription by RNA polymerase proceeds through a DNA-scrunching mechanism. *Science* **314**, 1144-7 (2006).
74. Revyakin, A., Liu, C., Ebright, R.H. & Strick, T.R. Abortive initiation and productive initiation by RNA polymerase involve DNA scrunching. *Science* **314**, 1139-43 (2006).
75. Tang, G.Q., Roy, R., Ha, T. & Patel, S.S. Transcription initiation in a single-subunit RNA polymerase proceeds through DNA scrunching and rotation of the N-terminal subdomains. *Mol Cell* **30**, 567-77 (2008).
76. Mukhopadhyay, J. et al. Translocation of sigma(70) with RNA polymerase during transcription: fluorescence resonance energy transfer assay for movement relative to DNA. *Cell* **106**, 453-63 (2001).
77. Kim, S. et al. High-throughput single-molecule optofluidic analysis. *Nat Methods* **8**, 242-5 (2011).
78. Lee, N.K. et al. Three-color alternating-laser excitation of single molecules: monitoring multiple interactions and distances. *Biophys J* **92**, 303-12 (2007).
79. Sobhy, M.A. et al. Versatile single-molecule multi-color excitation and detection fluorescence setup for studying biomolecular dynamics. *Rev Sci Instrum* **82**, 113702 (2011).
80. Morten, M.J. et al. Binding dynamics of a monomeric SSB protein to DNA: a single-molecule multi-process approach. *Nucleic Acids Research* **43**, 10907-10924 (2015).
81. Doose, S., Neuweiler, H., Barsch, H. & Sauer, M. Probing polyproline structure and dynamics by photoinduced electron transfer provides evidence for deviations from a regular polyproline type II helix. *Proc Natl Acad Sci U S A* **104**, 17400-5 (2007).
82. Sherman, E. & Haran, G. Fluorescence correlation spectroscopy of fast chain dynamics within denatured protein L. *Chemphyschem* **12**, 696-703 (2011).
83. Neuweiler, H. & Sauer, M. Using photoinduced charge transfer reactions to study conformational dynamics of biopolymers at the single-molecule level. *Curr Pharm Biotechnol* **5**, 285-98 (2004).
84. Haenni, D., Zosel, F., Reymond, L., Nettels, D. & Schuler, B. Intramolecular distances and dynamics from the combined photon statistics of single-molecule FRET and photoinduced electron transfer. *J Phys Chem B* **117**, 13015-28 (2013).

bioRxiv preprint doi: https://doi.org/10.1101/047779; this version posted May 11, 2016. The copyright holder for this preprint (which was not certified by peer review) is the author/funder. All rights reserved. No reuse allowed without permission.

85. Hamdan, S.M. et al. A unique loop in T7 DNA polymerase mediates the binding of helicase-primase, DNA binding protein, and processivity factor. *Proceedings of the National Academy of Sciences of the United States of America* **102**, 5096-5101 (2005).
86. Rasnik, I., McKinney, S.A. & Ha, T. Nonblinking and longlasting single-molecule fluorescence imaging. *Nat Methods* **3**, 891-893 (2006).
87. Cordes, T., Vogelsang, J. & Tinnefeld, P. On the Mechanism of Trolox as Antiblinking and Antibleaching Reagent. *Journal of the American Chemical Society* **131**, 5018-5019 (2009).
88. Campos, L.A. et al. A photoprotection strategy for microsecond-resolution single-molecule fluorescence spectroscopy. *Nature Methods* **8**, 143-146 (2011).
89. Lakowicz, J. Principles of fluorescence spectroscopy. 3rd edn Springer. *New York* (2006).
90. Iqbal, A. et al. Orientation dependence in fluorescent energy transfer between Cy3 and Cy5 terminally attached to double-stranded nucleic acids. *Proceedings of the National Academy of Sciences* **105**, 11176-11181 (2008).
91. van der Velde, J.H.M. et al. Mechanism of Intramolecular Photostabilization in Self-Healing Cyanine Fluorophores. *ChemPhysChem* **14**, 4084-4093 (2013).
92. Krstajić, N., Levitt, J., Poland, S., Ameer-Beg, S. & Henderson, R. 256 × 2 SPAD line sensor for time resolved fluorescence spectroscopy. *Optics Express* **23**, 5653-5669 (2015).
93. van der Velde, J.H.M. et al. Mechanism of intramolecular photostabilization in self-healing cyanine fluorophores. *ChemPhysChem* **14**, 4084-4093 (2013).
94. Gouridis, G. et al. Conformational dynamics in substrate-binding domains influences transport in the ABC importer GlnPQ. *Nat Struct Mol Biol* **22**, 57-64 (2015).
95. Ploetz, E. et al. PIFE meets FRET - a molecular ruler goes 2D. (2016).
96. Eggeling, C. et al. Data registration and selective single-molecule analysis using multi-parameter fluorescence detection. *Journal of Biotechnology* **86**, 163-80 (2001).
97. Nir, E. et al. Shot-noise limited single-molecule FRET histograms: comparison between theory and experiments. *J Phys Chem B Condens Matter Mater Surf Interfaces Biophys* **110**, 22103-24 (2006).
98. Press, W.H., S. A. Teukolsky, W. T. Vetterling, and B. P. Flannery. *Numerical recipes in C : the art of scientific computing*, xxvi, 994 (Cambridge University Press, Cambridge, U.K., 1992).